Research Paper

Identifying lncRNA–miRNA–mRNA networks to investigate Alzheimer's disease pathogenesis and therapy strategy

Nana Ma[1], Changrui Tie[1], Bo Yu[2,3], Wei Zhang[1,*], Jun Wan[1,4,*]

[1]Shenzhen Key Laboratory for Neuronal Structural Biology, Biomedical Research Institute, Shenzhen Peking University - The Hong Kong University of Science and Technology Medical Center, Shenzhen 518000, Guangdong Province, China
[2]Shenzhen Key Laboratory for Translational Medicine of Dermatology, Biomedical Research Institute, Shenzhen Peking University - The Hong Kong University of Science and Technology Medical Center, Shenzhen 518000, Guangdong Province, China
[3]Department of Dermatology, Peking University Shenzhen Hospital, Shenzhen 518000, Guangdong Province, China
[4]Division of Life Science, The Hong Kong University of Science and Technology, Kowloon, Hong Kong 999077, China
*Equal contribution

Correspondence to: Jun Wan, Wei Zhang; **email:** wanj@ust.hk, zhangweispace@163.com
Keywords: Alzheimer's disease (AD), ceRNA network, APP/PS1 mouse, RNA-sequencing, lncRNA
Received: September 27, 2019 **Accepted:** January 19, 2020 **Published:** February 7, 2020

ABSTRACT

Alzheimer's disease (AD), the most common cause of dementia, leads to neuronal damage and deterioration of cognitive functions in aging brains. There is evidence suggesting the participation of noncoding RNAs in AD-associated pathophysiology. A potential linkage between AD and lncRNA-associated competing endogenous RNA (ceRNA) networks has been revealed. Nevertheless, there are still no genome-wide studies which have identified the lncRNA-associated ceRNA pairs involved in AD. For this reason, deep RNA-sequencing was performed to systematically investigate lncRNA-associated ceRNA mechanisms in AD model mice (APP/PS1) brains. Our results identified 487, 89, and 3,025 significantly dysregulated lncRNAs, miRNAs, and mRNAs, respectively, and the most comprehensive lncRNA-associated ceRNA networks to date are constructed in the APP/PS1 brain. GO analysis revealed the involvement of the identified networks in regulating AD development from distinct origins, such as synapses and dendrites. Following rigorous selection, the lncRNA-associated ceRNA networks in this AD mouse model were found to be mainly involved in synaptic plasticity as well as memory (*Akap5*) and regulation of amyloid-β (Aβ)-induced neuroinflammation (*Klf4*). This study presents the first systematic dissection of lncRNA-associated ceRNA profiles in the APP/PS1 mouse brain. The identified lncRNA-associated ceRNA networks could provide insights that facilitate AD diagnosis and future treatment strategies.

INTRODUCTION

Alzheimer's disease (AD) was first described in 1906, which was recognized as a common cause of dementia and a major cause of death 70 years later [1]. Although AD has become a significant focus of research, the molecular mechanisms underlying its pathogenesis remain largely unknown [2]. At present, there are no effective prognostic biomarkers yet. Therefore, it is significant to identify not only the potential biomarkers for prediction of survival in this disease, but also the novel targets for prognosis improvement and guidance on the optimal individual treatment.

It was reported that 80% of the human genome is transcribed as noncoding RNAs (ncRNAs) [3], which can manipulate most of the potential biological functions [4]. Over the past two decades, it was demonstrated that ncRNAs, with their specific spatiotemporal expression patterns across various species, are extensively involved in numerous biological processes, including epigenetic regulation, chromatin remodeling, transcription control, and posttranscriptional processing [5]. More and more ncRNAs have been identified for their important roles in the pathogenesis of neurodegenerative disorders.

NcRNAs include microRNAs (miRNAs, ~20 nucleotides in length) and long noncoding RNAs (lncRNAs, larger than 200 nucleotides in length), which play significant roles in the regulation of various biological functions [6]. There is evidence that miRNAs and lncRNAs participate in AD pathophysiology, which includes the formation and development of β-amyloid (Aβ) plaques, neurofibrillary tangles, synaptic loss and neuronal death [7–9]. The ncRNAs have been detected by RNA-sequencing (RNA-seq) or microarrays in many organisms, which presents exciting implications for understanding the regulation of basic biological systems and pathophysiological conditions, as well as the development of new therapeutic treatment of many diseases [10].

LncRNAs modulate the nervous system in various biological dimensions, including epigenetic regulation [11, 12] and posttranscriptional regulation [13]. For example, β-site amyloid precursor protein (APP)-cleaving enzyme 1-antisense (BACE1-AS) stabilizes BACE1 RNA and promotes APP cleavage, which is actively involved in the pathogenesis of Alzheimer's disease [6, 9]. Evf2 RNA controls adult hippocampal neurogenesis through regulating dynamic expression of downstream targets [14]. Both HOTAIR [6] and MALAT1 [15] RNAs are upregulated in brain tumors and promote tumor metastasis. Malat1 RNA regulates synaptogenesis in mouse hippocampal neurons through controlling gene expression [16].

Recent studies suggest that lncRNAs, circRNAs, pseudogenes and mRNAs may function as miRNA sponges [17–19]. They compete with each other through miRNA response elements (MREs) and modulate the progress of many diseases [20, 21] including AD [9, 6, 13]. In addition to post-transcriptional regulation, epigenetic modifications may also play a crucial role in AD pathogenesis [7, 22]. These refined and complicated regulatory networks may help to explain why the isolation of a single component (e.g., β-secretase and apolipoprotein E4) failed to fully account for the whole pathogenesis process of AD [23]. It suggests that the underlying mechanisms for the involvement of competing endogenous RNA (ceRNA) in AD remain to be determined.

The rational strategy to gain insight into neurodegenerative diseases such as AD would make the study of lncRNA-associated ceRNA networks comprehensively. The elucidation of lncRNA-associated ceRNA networks in AD might help to develop new therapeutic targets for AD. In APP/PS1 mice which express APP695swe and PS1-dE9 mutations, Aβ can be detected in 6-month old mice, and then extracellular Aβ deposits in the cortex are apparent in 9-month old mice. Moreover, synaptic transmission and long-term potentiation are clearly impaired in 9-month old mice [24]. Thus, deep RNA-seq was performed in this study to find lncRNA-associated ceRNA networks in the brain of APP/PS1 mice together with the wild-type (WT) control mice at the 6- and 9-month-old stages. RNA-seq is widely used to determine the differential gene-expression profiles that underlie phenotypic differences [25, 26]. The data by RNA-seq identifies lncRNA-associated ceRNA networks in the APP/PS1 mouse model of AD (Figure 1), which can contribute to the development of new therapeutic targets and novel diagnostic methods for AD.

RESULTS

Overview of lncRNA and mRNA-seq data

A total of 1,145,853,722 raw reads were generated. 317,603,558 raw reads and 276,260,804 raw reads were generated for 6-month-old WT and APP/PS1 mice respectively, while 286,203,120 raw reads and 265,786,240 raw reads were generated for 9-month-old WT and APP/PS1 mice respectively. After discarding the reads with adapters, poly-N > 10%, or any other potential contaminants, 1,119,187,680 clean reads were obtained. 311,741,312 clean reads and 266,033,410 clean reads were obtained for 6-month-old WT and APP/PS1 mice respectively, while 278,938,832 clean reads and 262,474,126 clean reads were obtained for 9-month-old WT and APP/PS1 mice respectively. Both reference genome and gene model annotation files were downloaded directly from the genome website. An index of the reference genome was constructed with bowtie2 v2.2.8, and paired-end clean reads were aligned to the reference genome with HISAT2 v2.0.4 [27]. HISAT2 was run with "--rna-strandness RF," while other parameters were set as default. Especially the mapping rates was 91.53% and 91.74% for APP/PS1 and WT mice, respectively. The transcripts were filtered out with coding potential prediction with the function of CNCI (Coding-Non-Coding-Index) (v2) [28], CPC (Coding Potential Calculator) (0.9-r2) [29], PfamScan (v1.3)

[30], and PhyloCSF (phylogenetic codon substitution frequency) (v20121028) [31]. 9,299 lncRNAs (including 2,463 annotated lncRNA and 6,836 novel lncRNA) and 48,718 protein-coding transcripts (mRNA) were identified and used for subsequent analyses.

Overview of miRNA-seq data

A total of 99,137,837 raw reads were generated. 28,672,205 raw reads and 20,760,197 were generated for 6-month-old WT and APP/PS1 mice respectively, while 23,016,993 raw reads and 26,688,442 raw reads were generated for 9-month-old WT and APP/PS1 mice respectively. After the removal of low quality and adapter sequences, 96,028,757 clean reads were obtained. 27,710,151 clean reads and 20,281,596 clean reads were obtained for 6-month-old WT and APP/PS1 mice respectively, while 22,393,001 clean reads and 25,644,009 clean reads were obtained for 9-month-old WT and APP/PS1 mice respectively. These clean reads were filtered by length (18–35 nucleotides), and a majority of the selected reads for both groups were 22 nucleotides in length. The selected reads were then mapped to the mouse reference sequence with Bowtie [32], and the mapping rate was 94.61% and 94.78% for APP/PS1 and WT mice respectively. Then, the mapped tags were then annotated and classified by alignment with noncoding small RNAs (including rRNA, tRNA, small nuclear RNA, and small nucleolar RNA), repeat-associated RNA, exon- and intron-associated RNAs in GenBank before sequenced in the miRBase v.20.0. In addition, both miREvo [33] and miRDeep2 [34] software was used to predict previously unidentified miRNAs. Ultimately, 1,411 mature miRNAs (1,312 known and 99 previously unknown) were detected and used for subsequent analyses.

Differential expression analysis: APP/PS1 versus WT

283 significantly dysregulated lncRNA transcripts (including 170 upregulated transcripts and 113 down-regulated transcripts) were identified in the 6-month-old APP/PS1 mice (Figure 2A, Supplementary Table 1), while 254 significantly dysregulated lncRNA transcripts (including 144 upregulated transcripts and 110 downregulated transcripts) were identified in the 9-month-old APP/PS1 mice (Figure 2B, Supplementary Table 2). A heatmap was constructed to visualize the cluster analysis results of the lncRNAs expression (Figure 2C). Then based on the transcripts per million

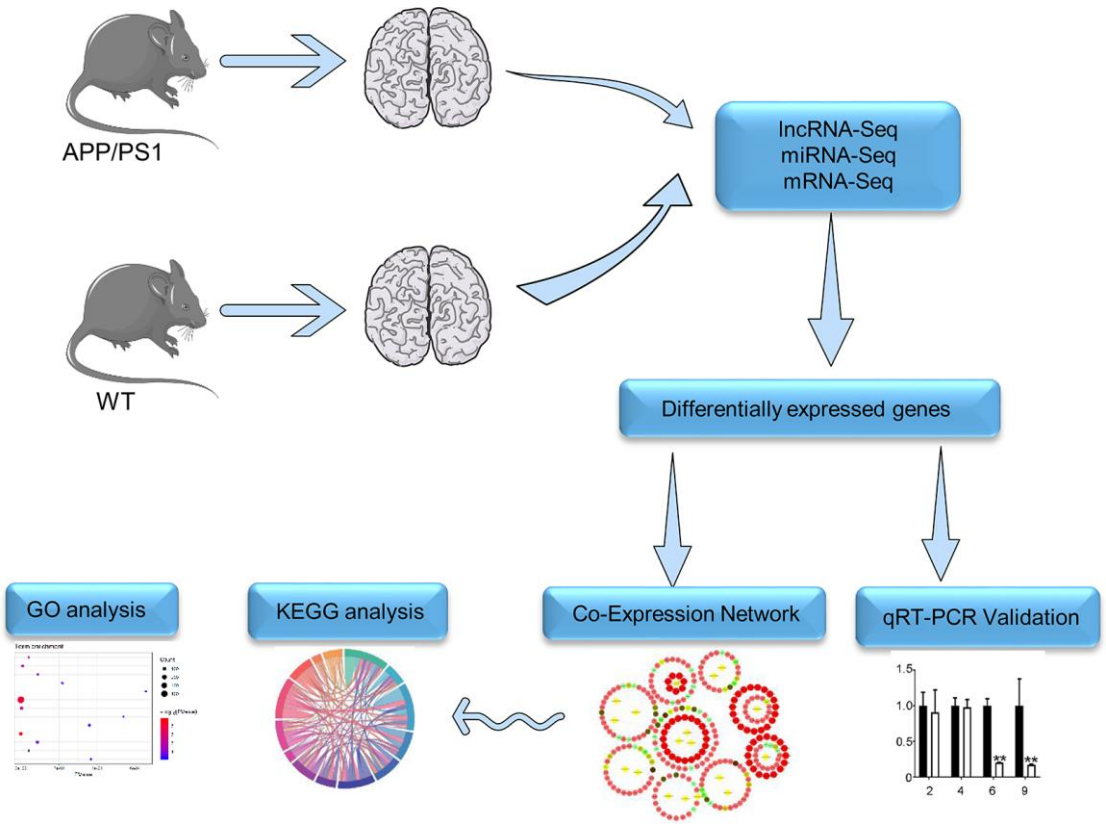

Figure 1. The workflow of RNA-seq. Details of the methods used for mRNA-seq, miRNA-seq, and lncRNA-seq are described in Supplementary Materials.

(TPM) values, 32 significantly dysregulated miRNAs were identified between the 6-month-old groups, which included 9 upregulated miRNAs and 23 downregulated miRNAs in APP/PS1 mice (Figure 2D, Supplementary Table 3). 42 miRNAs were significantly dysregulated between the 9-month-old groups, which included 20 upregulated miRNAs and 22 downregulated miRNAs in APP/PSI mice (Figure 2E, Supplementary Table 4). The cluster analysis of miRNAs expression was performed, and then a heatmap was generated (Figure 2F). Finally, the FPKM values (fragments per kilobase of exons per million fragments mapped) were used to estimate the expression levels of mRNA transcripts. 310 mRNA transcripts were significantly dysregulated, including 132 upregulated transcripts and 178 downregulated transcripts in APP/PS1 mice at 6 months (Figure 2G, Supplementary Table 5), while 226 mRNAs were significantly dysregulated, with 108 and 118 upregulated and downregulated in APP/PS1 mice at 9 months (Figure 2H, Supplementary Table 6). Once, cluster analysis for the expression of mRNAs was performed and a heatmap was generated (Figure 2I).

qPCR validation

The differential expression identified by RNA-seq experiments were confirmed with qPCR. 24 differentially expressed transcripts were randomly selected, including 6 lncRNAs, 9 miRNAs and 9 mRNAs. All of the selected transcripts were detected in the brain of 2–9-month-old APP/PS1 and WT mice. Besides, there was statistical difference between the two groups (Figures 3–5). Overall, the qPCR results were highly consistent with the RNA-seq data.

Construction of lncRNA-associated ceRNA networks

According to the ceRNA hypothesis, the ceRNAs can compete for the same MREs in regulatory networks. In this study, RNA-seq data were used to map ceRNA networks in the APP/PS1 brain for the first time. The differentially expressed transcripts (lncRNAs, miRNAs, and mRNAs) were split into three groups depending on the expression patterns. The 6yes9no group included transcripts differential expressed at 6 months but not differential expressed at 9 months of age, play a role in AD pathogenesis; The 6no9yes group included transcripts not differential expressed at 6 months but differential expressed at 9 months, participate in the development of AD; The 6yes9yes group included transcripts differential expressed at both 6 and 9 months, which contributed to in all stages of AD (Figure 6A).

6yes9no group included a total of 148 lncRNAs and 376 mRNAs that were differentially expressed and shared common MRE binding sites from 33 significantly dysregulated miRNAs (Supplementary Tables 7, 8). 6no9yes significantly dysregulated group included a total of 135 lncRNAs, 526 mRNAs, and 50 miRNAs (Supplementary Tables 9, 10). Besides, 7 lncRNAs, 31 mRNAs and 2 miRNA were included in 6yes9yes group (Supplementary Table 11). The ceRNA networks included both positive and negative regulation (Figures 6, 7). Figure 6 shows the increased lncRNAs, decreased miRNAs and increased mRNAs in APP/PS1 mice, while Figure 7 shows the decreased lncRNAs, increased miRNAs, and decreased mRNAs in APP/PS1 mice. It indicated potential critical RNA interactions involved in AD pathogenesis.

Gene Ontology (GO) and Kyoto Encyclopedia of Genes and Genomes (KEGG) pathway analyses

A lncRNA-associated ceRNA network can alter the regulation of related mRNA-encoding genes. GO analyses were performed on the genes included in the networks identified here and several GO terms were found to be significantly enriched (Supplementary Tables 12–14). The GO terms included biological process (BP), cellular component (CC), and molecular function (MF), as shown in Figure 8. The top highly enriched terms were cytoskeleton (GO:0005856), postsynaptic density (GO:0014069), cell-cell adherens junction (GO:0005913) and dendrite (GO:0030425). A number of cognition-associated terms were also observed, such as axon (GO:0030424), synapse (GO:0045202), postsynaptic density (GO:0014069), intracellular signal transduction (GO:0035556), and neuron projection (GO:0043005). Noteworthy, the enriched GO terms for 6yes9no group were different from those for 6no9yes group, which suggested the expression changes in the functional genes during the progression of disease. For example, the Go pathways "transferase activity" was found in the "Molecular function" section of both B and C, but not in A of the Figure 8. It was explained that AD is characterized by the accumulation of intracellular and extracellular proteins, including the microtubule-associated protein Tau and the decomposition product of amyloid precursor protein β-amyloid Aβ. Tissue-type trans-glutaminase (tTG) is a calcium-dependent enzyme that catalyzes the cross-linking of proteins to generate isomeric peptides of the γ-glutamyl-ε-lysine structure (representing transferase activity). This covalent attachment results in protein aggregation and deposition due to its strong resistance to proteolysis. In previous studies it was demonstrated that the protein levels of tTG and isopeptides were increased in the brain of patients with advanced AD, and the activity increases noticeably with age. These findings suggest that tTG may be an important cause of abnormal protein

accumulation in advanced AD pathology, which may not have been changed in the early stages [35, 36]. Consequently, 6yes9no group is not enriched in this pathway. In summary, the lncRNA-associated ceRNA networks might participate in the pathological progression of AD at distinct stages through different mechanisms. The establishment of these networks helps to investigate the functions of the key genes in AD and to guide determination of the regulatory mechanisms between the components of the ceRNA network.

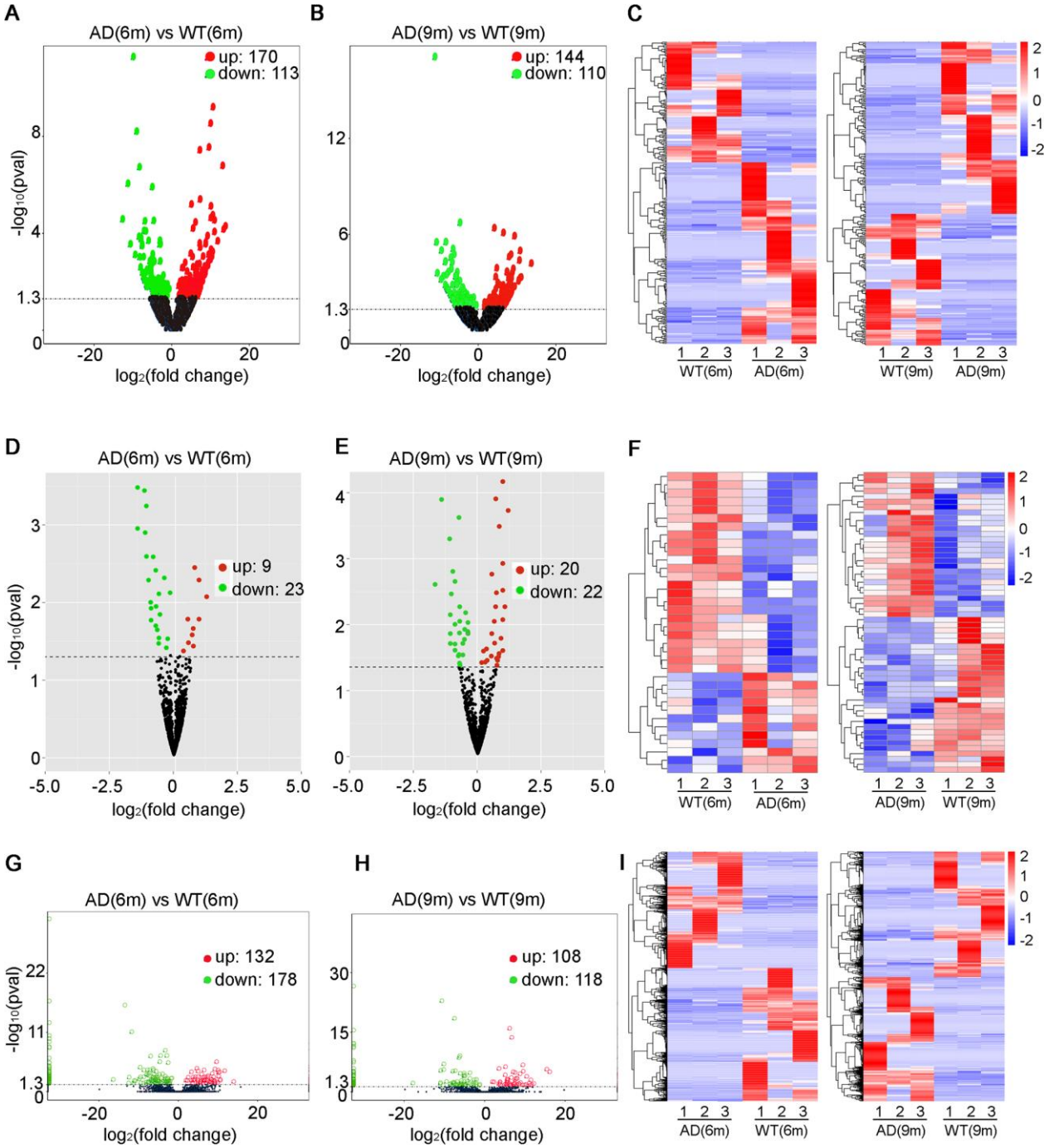

Figure 2. Expression profiles of distinct RNAs. (**A**–**C**) Expression profiles of lncRNAs. (**A**, **B**) In the volcano plots, green, red, and black points represent lncRNAs that were downregulated, upregulated, and not significantly different in APP/PS1 mice relative to wild-type (WT) control mice at 6 and 9 months, respectively. x-axis: log2 ratio of lncRNA expression levels between AD and WT. y-axis: false-discovery rate values (-log10 transformed) of lncRNAs, P<0.05 (**C**) Cluster analysis of expression of lncRNAs. Red and blue: increased and decreased expression at 6 and 9 months, respectively. Expression profiles are similarly shown for (**D**–**F**) miRNAs, p<0.04 and (**G**–**I**) mRNAs, q<0.05.

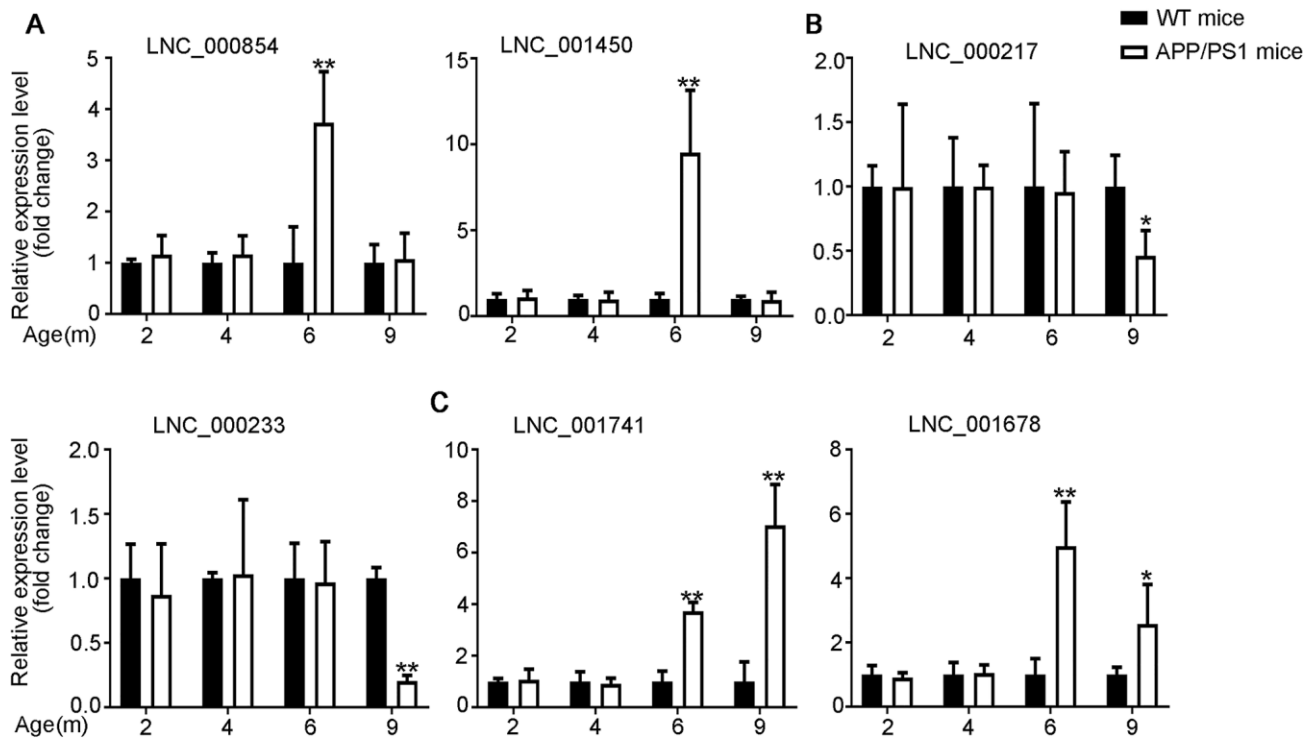

Figures 3. Validation of expression of lncRNAs by using qPCR. The identified differentially expressed transcripts (lncRNAs, miRNAs, and mRNAs) were divided into three groups. (**A**) 6yes9no group represents transcripts differential expressed at 6 months but not at 9 months; (**B**) 6no9yes group represents transcripts not differential expressed at 6 months but differential expressed at 9 months; (**C**) 6yes9yes group represents transcripts differential expressed at both 6 and 9 months. The expression of lncRNAs was quantified relative to *Gapdh* expression level by using the comparative cycle threshold (ΔCT) method. Data are presented as means ± SD (n = 3, *p < 0.05, **p < 0.01).

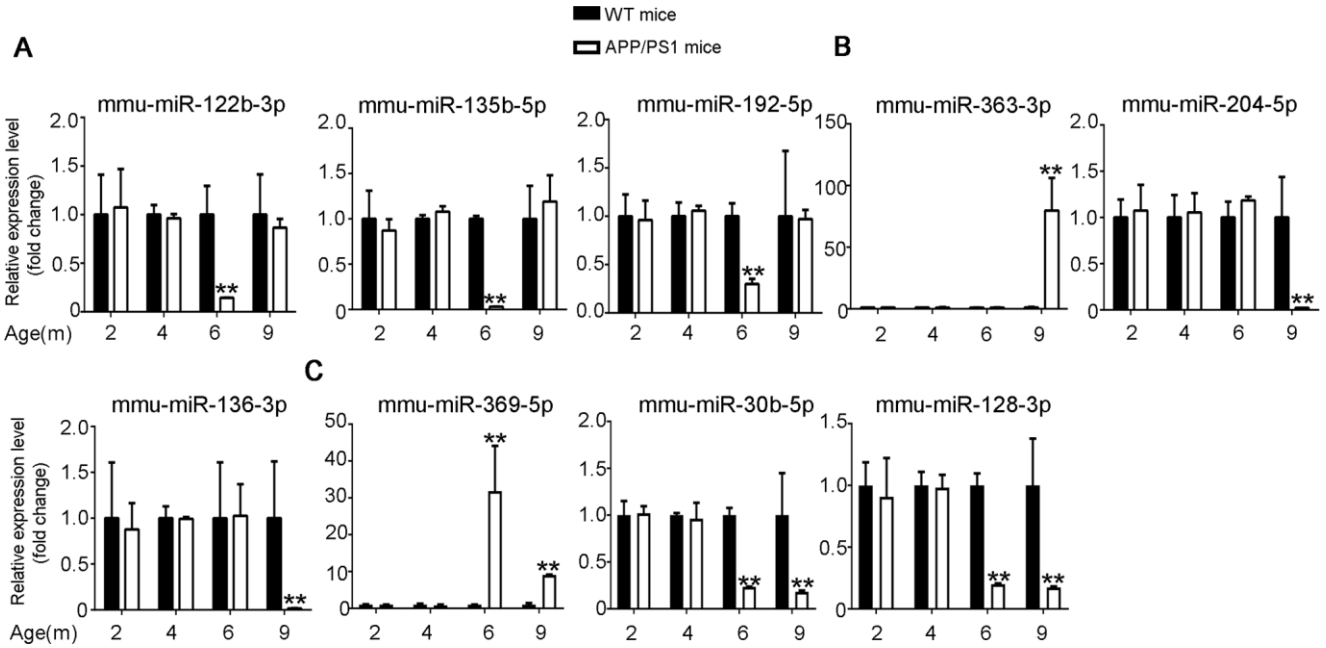

Figures 4. Validation of miRNA expression by using qPCR. (**A**) 6yes9no group, (**B**) 6no9yes group, and (**C**) 6yes9yes group. The expression levels of miRNAs were quantified relative to *U6* expression level by using the comparative cycle threshold (ΔCT) method. Data are presented as means ± SD (n = 3, *p < 0.05, **p < 0.01).

KEGG pathway analysis was conducted to determine the signaling cascades related to the identified genes. By using $p < 0.05$ as the threshold value, a number of significantly enriched pathways were identified (Figure 9, Supplementary Tables 12–14), including neuroactive ligand-receptor interaction, AMP-activated protein kinase (AMPK) signaling, long-term potentiation, Hippo signaling, glutamatergic synapse, PI3K-Akt signaling, insulin secretion, focal adhesion and axon guidance.

Association study

We selectively analyzed the data for lncRNAs and miRNAs of which the target genes significant differential expressed between APP/PS1 and WT mice (corrected $p < 0.05$). Additionally, we also selected lncRNAs and miRNAs of which the target genes showed enrichment in the mouse brain and were associated with AD. Analyses were performed to investigate the relationships between lncRNA-associated ceRNA networks and AD. For example, LNC_000854, LNC_001450, LNC_001451, LNC_001887, LNC_002205, LNC_002746, LNC_003197, LNC_003206, LNC_003458, LNC_004148, LNC_004514, LNC_004707 and LNC_006482 were identified as ceRNAs of mmu-miR-122-5p, which targets *Klf4*. The expression of *Klf4* was higher in AD mice than in WT mice. *Klf4* regulates amyloid-β (Aβ)-induced neuroinflammation and plays a potential role in not only oligomeric Aβ42-induced neurotoxicity but also the pathogenesis of Alzheimer's disease [37]. LNC_000033 was found to be a ceRNA of mmu-miR-128-2-5p,

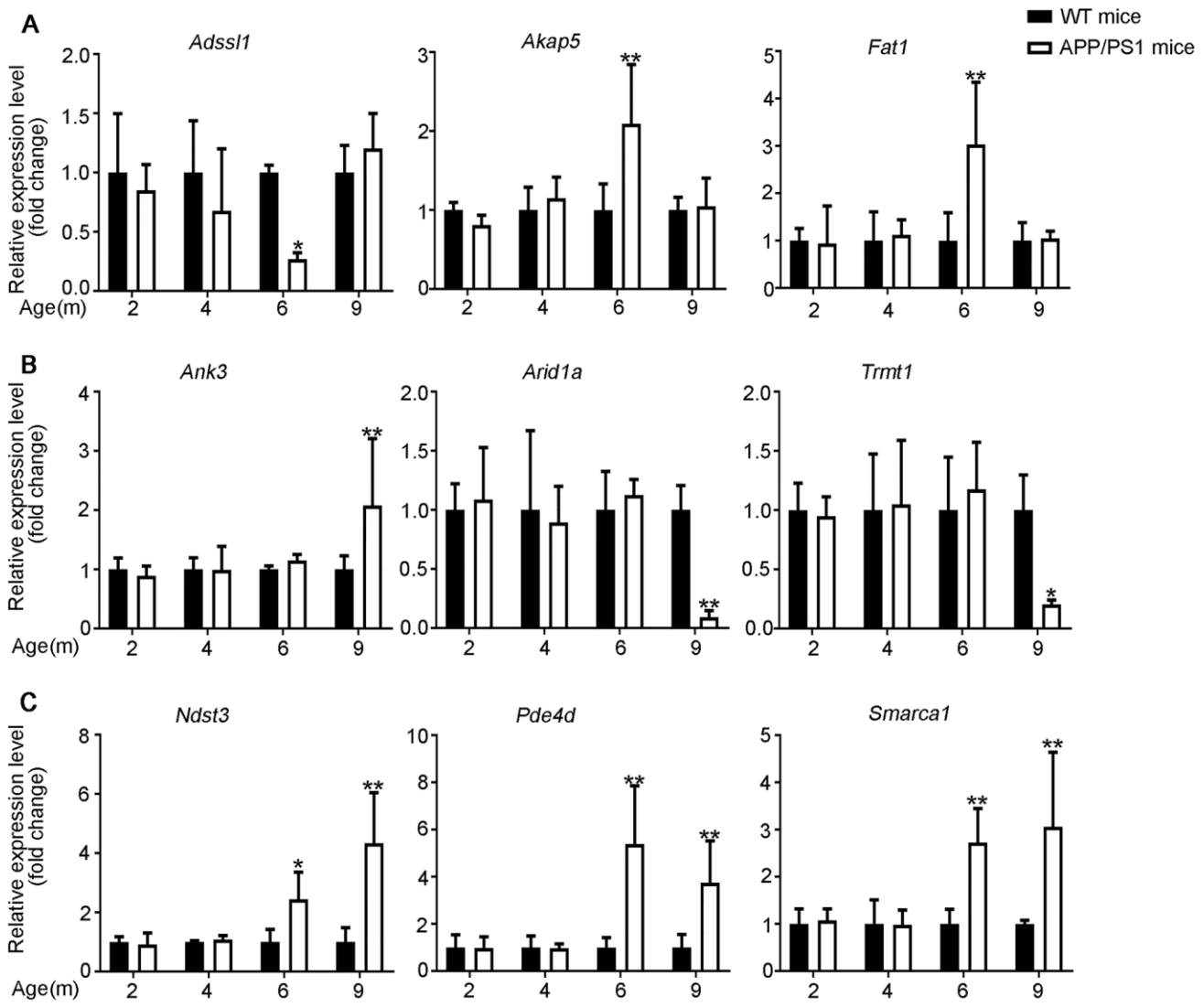

Figures 5. Validation of mRNA expression by using qPCR. (**A**) 6yes9no group, (**B**) 6no9yes group, and (**C**) 6yes9yes group. The mRNA expression was quantified relative to *Gapdh* expression level by using the comparative cycle threshold (ΔCT) method. Data are presented as means ± SD (n = 3, *p < 0.05, **p < 0.01).

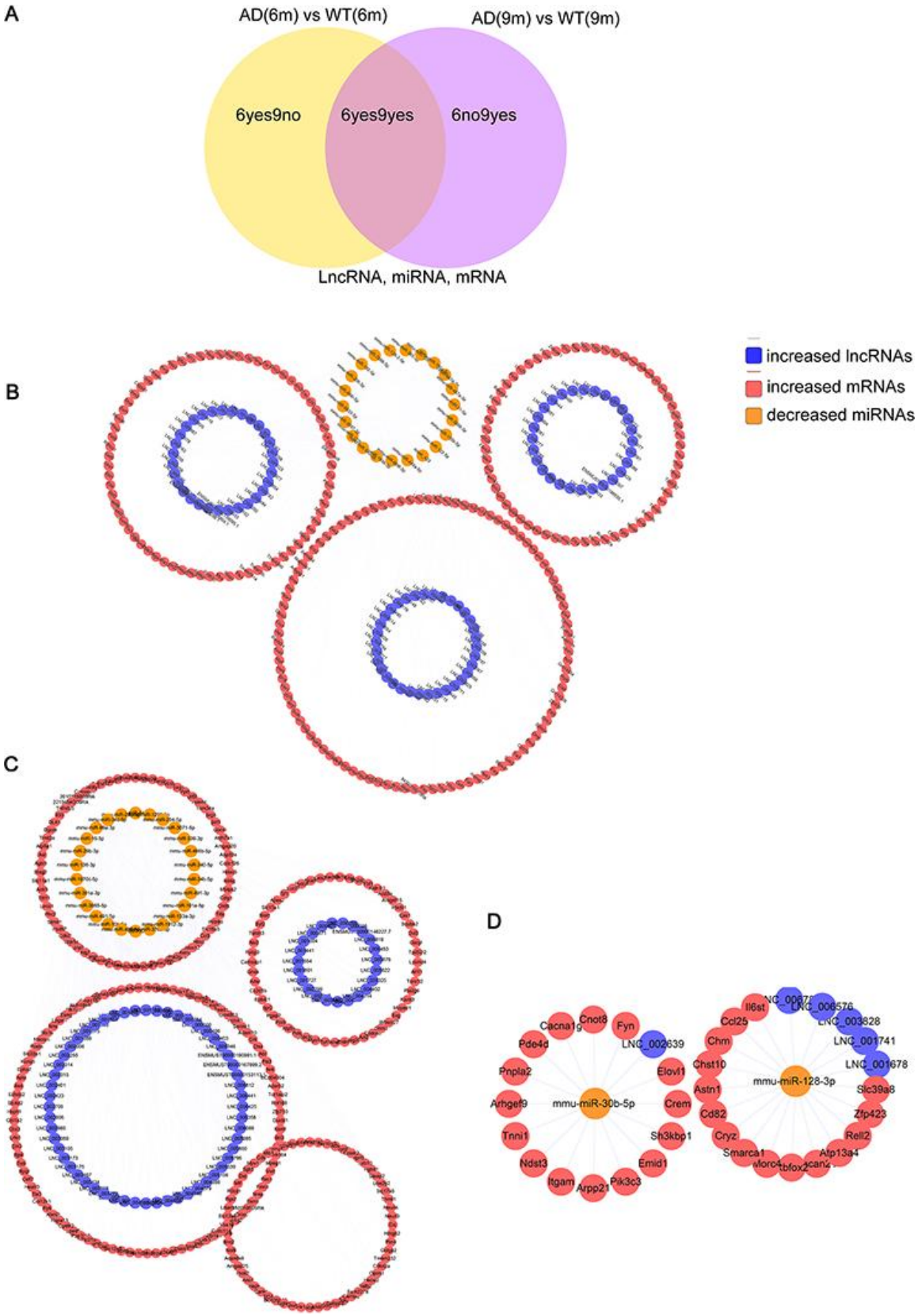

Figure 6. The lncRNA-associated ceRNA networks in APP/PS1 mice. CeRNA networks were constructed based on identified lncRNA–miRNA and miRNA–mRNA interactions. The networks include increased lncRNAs, decreased miRNAs, and increased mRNAs in APP/PS1 mice. (**A**) Grouping (**B**) 6yes9no group, (**C**) 6no9yes group, and (**D**) 6yes9yes group.

mmu-miR-135b-5p, mmu-miR-3097-3p, mmu-miR-31-5p, and mmu-miR-449a-5p, which target *Synpo*. *Synpo* was upregulated in the sequencing data. *Synpo* have been identified as crucial components in dendritic spine plasticity of the developing hippocampus. The disorder of *Synpo* expression affected the development of dendritic spines [38–42], which might also affect the early stages of AD. In addition, our analysis also revealed that miRNAs may act directly on their target genes. For example, *Grsf1*, targeted by mmu-miR-187-3p, mmu-miR-363-3p and mmu-miR-7004-5p, could be essential for the development of embryonic brain [43]. The additional results are listed in Supplementary Tables 7–11. Overall, it suggested that the identified lncRNA-associated ceRNA networks may be involved in the regulation of AD.

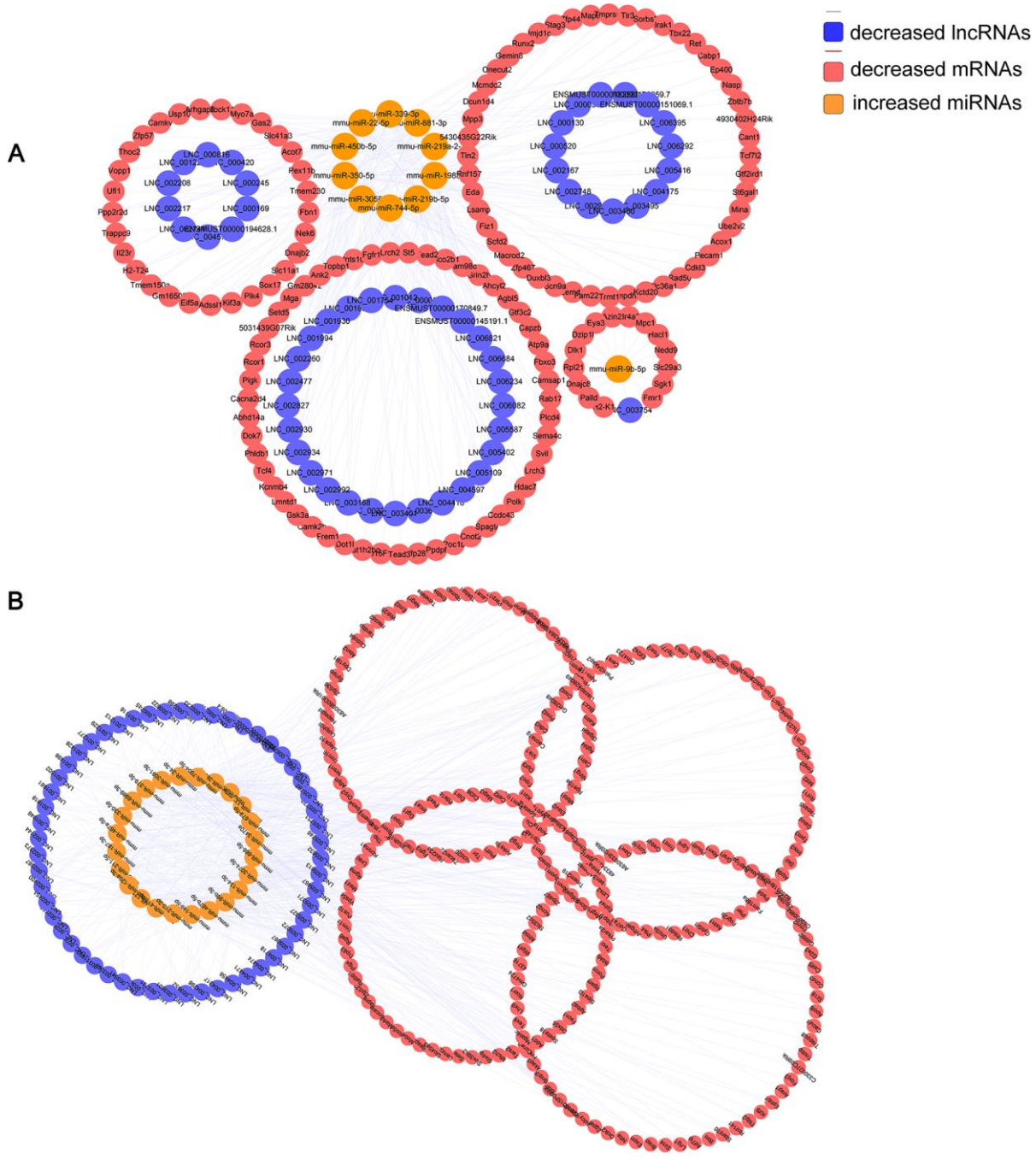

Figure 7. Identified lncRNA-associated ceRNA networks in APP/PS1 mice. The ceRNA networks were constructed based on identified lncRNA–miRNA and miRNA–mRNA interactions. The networks include decreased lncRNAs, increased miRNAs, and decreased mRNAs in APP/PS1 mice. (**A**) 6yes9no group, and (**B**) 6no9yes group.

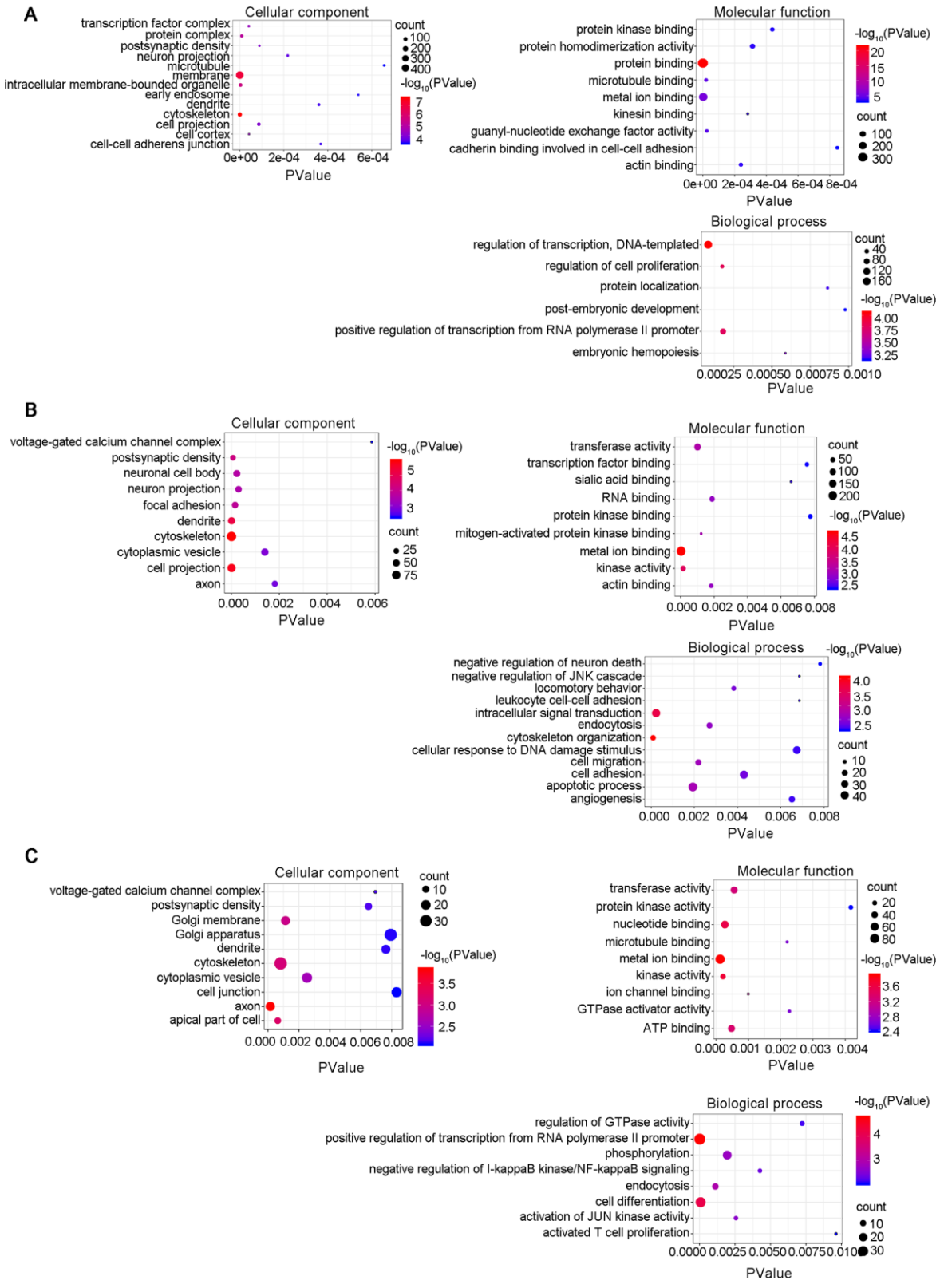

Figure 8. Gene Ontology (GO) enrichment annotations of the pathological progression of AD: biological process, cellular component, molecular function. The top terms were synapse (GO:0045202), cytoskeleton (GO:0005856), postsynaptic density (GO:0014069), cell-cell adherens junction (GO:0005913), dendrite (GO:0030425), axon (GO:0030424), and neuron projection (GO:0043005). (**A**) 6yes9no group, (**B**) 6no9yes group, and (**C**) 6yes9yes group. Significantly enriched GO pathways were defined as p values of <0.01. GO analysis was conducted with DAVID (https://david.ncifcrf.gov/summary.jsp) database.

DISCUSSION

AD is the most common neurodegenerative disease, of which the exact pathologic mechanism remains unknown. Although the traditional research tools and expertise detect some early brain changes of AD, additional research technologies remains necessary to fine-tune the accuracy of these tools. Recently, several studies on AD have focused on the epigenetic regulation of AD pathogenesis and identified the potential targets for therapy. lncRNAs expressed in brains have been reported to be contributory to the pathophysiology of AD [44, 45]. However, the roles of the lncRNAs in AD have remained mostly unknown.

MiRNAs are 22-nucleartide-long ncRNAs that can induce target gene silencing through complementary base-pairing with MREs on their 3′ UTRs and recruitment of RNA induced silencing complex (RISC) [46]. A total of 519 canonical miRNA genes have been identified in the human genome [47, 48]. There are roughly 70% of the identified miRNAs expressed in the provisional brain and in neurons [49], which suggests that miRNAs perform critical regulatory functions in the development of central nervous system (CNS), the formation of dendritic spine, neurite outgrowth, as well as neuronal differentiation and maintenance. The deregulation of miRNA is involved in neurodegenerative disorders such as AD and Parkinson's disease (PD) [6], as well as in psychiatric disorders such as schizophrenia [50]. For example, let-7, miR-15a and miR-101 target APP, while miR-15a, miR-9 and miR-107 regulate BACE1 [8].

Over the past several years, the ceRNA hypothesis has been validated by numerous experiments. So far, ceRNA mechanisms and network construction have been mainly studied in the field of cancer research [51–54]. Only a small number of ceRNA interactions have been reported to be associated with neuro-degenerative disorders. Recently, researchers have started to explore the ceRNA regulatory mechanism for specific neurodegenerative disorders in a systematic manner. Nevertheless, exciting advances have been made in our understanding of ceRNA interactions in neurodegenerative disorders. In our previous study, the lncRNA-ceRNA network was constructed in the brain

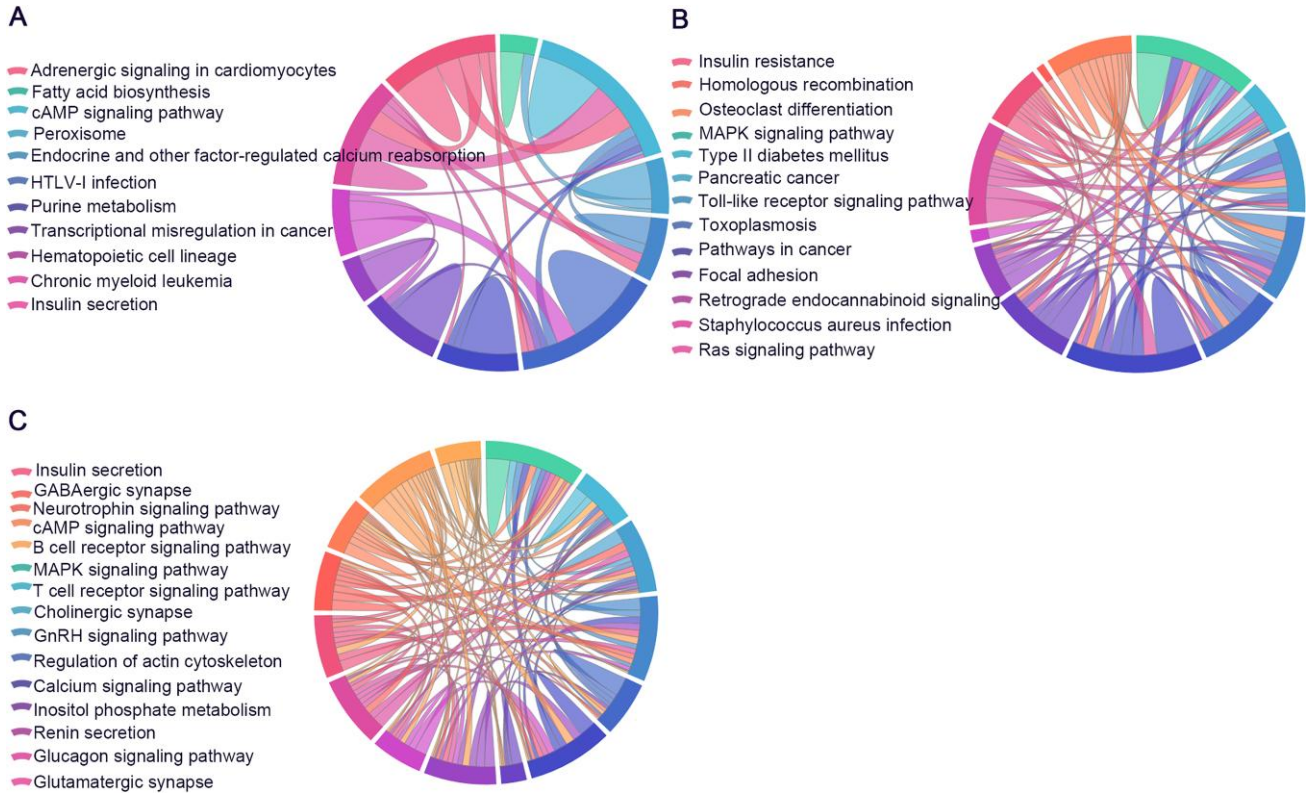

Figure 9. Significantly enriched Kyoto Encyclopedia of Genes and Genomes (KEGG) and Reactome pathways. The identified lncRNA-associated ceRNA-network genes participate in distinct aspects of AD pathology. (**A**) 6yes9no group, (**B**) 6no9yes group, and (**C**) 6yes9yes group. Significantly enriched KEGG pathways with p values of <0.05. Each line represents a gene, and the number of lines indicates the genes enriched. KEGG analysis was conducted with DAVID (https://david.ncifcrf.gov/summary.jsp) database.

of 12-month-old APP/PS1 mice [55]. As the sequencing depth and coverage limit the amount of generated sequences, the compositions of networks are slightly different. However, the key pathways in AD have been discovered. In order to not only explore changes of the ceRNA networks in the early stages of AD but also identify the early biomarkers, lncRNA-ceRNAs networks were constructed in the brain of 6- and 9-month-old APP/PS1 mice.

So far, it is the first comprehensive high-throughput sequencing analysis of the expression profiles of lncRNA, miRNA and mRNA in the APP/PS1 mouse model of AD. The dysregulated lncRNAs, miRNAs and mRNAs exhibited significant differential expression between AD and WT control groups, which suggested that these transcripts are associated with the pathogenesis of AD. For example, *Fndc3b* is essential for proliferation, adhesion, spreading and migration of nerve cells [56]. *Trappc9*, another differential expressed gene, plays a critical role in the development of human brain, possibly through its effect on NF-kappaB activation and protein trafficking in the postmitotic neurons of the cerebral cortex [57]. *Acsl6* mRNA is highly enriched in the brain and acsl6-/- mice demonstrate motor impairments, altered glutamate metabolism, increased astrogliosis and microglia activation [58]. Mmu-miR-376a-5p is a pancreatic islet-specific miRNA that regulates insulin secretion as an important pathway for the development of AD [59], while mmu-miR-134 regulates the development of cortical neurons [60]. The level of mmu-miR-29 is also substantially reduced in AD patients and it acts to regulate BACE1 expression [61, 62]. The qRT-PCR experiment confirmed the profiles from the high-throughput sequencing data, which indicated the reliability of the sequencing data.

In our study, RNA-seq was used to systematically analyze lncRNA, miRNA and mRNA profiles in the brain of 6- and 9-month-old APP/PS1 mice. The transcripts of 6yes9no group might participate in AD pathogenesis, of which the stability and specific expression could make them suitable as optimal biomarkers for AD. The transcripts in 6no9yes group might function in the development of AD. It is worth noting that the transcripts in 6yes9yes group may be involved in the disease at all stages, which suggests that focus on these transcripts could facilitate the development of lncRNA-based diagnostic tools and therapeutic strategies for AD. Overall, lncRNA and miRNA molecules have a potential to act as key regulators AD in different aspects. Both lncRNAs and protein-coding mRNAs function as ceRNAs and super-sponges to regulate the expression of miRNA. Therefore, we predicted the miRNA–mRNA and miRNA–lncRNA interaction with miRanda and constructed DElncRNA–DEmiRNA–DEmRNA triple networks for APP/PS1 and WT mouse brain. The selected lncRNA-associated ceRNA networks may facilitate new insights into AD and contribute novel treatments for the disease.

We performed GO enrichment and KEGG analysis of the genes in the ceRNA networks and identified not only a number of enriched terms relevant to the pathological process of AD, including cytoskeleton (GO:0005856), cell adhesion (GO:0005913), dendrite (GO:0030425), postsynaptic density (GO:0014069), axon (GO:0030424), synapse (GO:0045202), and neuron projection (GO:0043005), but also various pathways, including MAPK signaling, insulin secretion, Type II diabetes mellitus, cAMP signaling, Hippo signaling, focal adhesion, dopaminergic synapse, and PI3K-Akt signaling pathways. Analysis of the data revealed several lncRNA-associated ceRNA networks that participate in AD. *Akap5* contributes to synaptic plasticity mediated by NMDARs and AMPA-type glutamate receptors (AMPARs) and plays a critical role in the progression of AD [21, 63, 64]. One of these networks involves the gene *Akap5* and the ceRNAs, including LNC_000217, LNC_000233, LNC_000622, LNC_001498, LNC_001502, LNC_001818, LNC_002144, LNC_002373, LNC_002451, LNC_002620, LNC_003852, LNC_004317, LNC_005072, and LNC_005613. These ceRNAs have the potential to bind mmu-miR-679-5p, which targets *Akap5*. The APP/PS1 mice used in this study cannot represent the whole disease, which is primarily related to β-amyloid toxicity. Therefore, further research is necessary to better understand the regulation of these networks in AD.

Our research is just the beginning so that there remain many challenges and problems to be solved in the future. The cumulative evidence has helped to refine the dynamic ceRNA regulation [20], which reveals that various factors could contribute to the creation of miRNA and ceRNA hierarchies. These factors can be summarized as follows: miRNA target-site efficacy; shared MRE abundance; miRNA/ceRNA expression level and subcellular localization [21]; miRNA: target ratio; competition between rate-limiting molecules, such as Ago [63]; and advanced ceRNA hierarchy strategies. Moreover, attempt was made to decode the complexity of ceRNA regulatory networks. After the initial establishment of the ceRNA network, the biological mechanisms and functions mediated by the ceRNA mechanism should be predicted and verified by means of in vivo experiments in the future.

For a long time, there has been widespread recognition that ncRNAs are incapable to encode proteins [64]. Nevertheless, with the advancement of deep ribosome profiling sequencing (Ribo-Seq) technology, mass

spectrometry and algorithms, a subset of ncRNA have been identified to encode peptides (<100 amino acids) or proteins, such as muscle-specific lncRNAs [65–67] and cancer-related lncRNA HOXB-AS3 [68]. At present, only few studies focused on Alzheimer's disease. Peptides/proteins encoded by ncRNAs might represent the drug targets or biomarkers for the prognosis of AD patients. Therefore, it's significant to summarize the characteristics of peptides/proteins encoded by ncRNAs and their outlook for small molecule peptide drugs, drug targets and biomarkers.

In conclusion, the brain lncRNA-associated ceRNA profiles of APP/PS1 and WT mice were clarified. Our findings improve the current understanding of ceRNA biology and the regulatory roles of these RNAs in the pathogenesis of AD. These new networks reveal the potential biomarkers and may offer a promising target for the development of drugs to treat AD.

MATERIALS AND METHODS

Tissue preparation

WT and APP/PS1 mice [originally from The Jackson Laboratory; strain B6.Cg-Tg(APPswe, PSEN1dE9) 85Dbo/Mmjax [43]] were purchased from the Model Animal Research Center of Nanjing University. The mice were housed one per cage under standard conditions (25°C, 50% humidity, a 12-hour light/dark cycle, and specific-pathogen-free environment). The mice were provided with free access to the standard diet until they met the age requirements (6 and 9 months). 3 AD and 3 wild-type male mice born in the same litter were used as experimental and control groups, of which cerebral cortex samples were collected for RNA-seq. All animal experiments were performed in accordance with animal use protocols approved by the Committee for the Ethics of Animal Experiments, Shenzhen Peking University, the Hong Kong University of Science and Technology Medical Center (SPHMC) (protocol number 2011-004).

RNA extraction and qualification

Total RNA from each sample was isolated with TRIzol reagent (Invitrogen) according to the manufacturer's instructions and separated on 1% agarose gels to assess RNA degradation and contamination. RNA purity was measured with a NanoPhotometer spectrophotometer (IMPLEN, CA, USA). RNA concentration was measured with a Qubit RNA Assay Kit in a Qubit 2.0 Fluorometer (Life Technologies, CA, USA). RNA integrity was evaluated with the RNA Nano 6000 Assay Kit of a Bioanalyzer 2100 System (Agilent Technologies, CA, USA).

RNA-seq

Details of the mRNA-seq, miRNA-seq, and lncRNA-seq methods are described in Supplementary Materials.

Expression analysis

We calculated the FPKM values of transcripts by using Cuffdiff (v.2.1.1) to evaluate the expression levels of protein-coding genes and lncRNA in each sample [69]. The expression levels of miRNAs were estimated as TPM values as described [69]. Transcripts with p values less than 0.05 were regarded as being differentially expressed between APP/PS1 and WT mice. Normalized expression = (mapped reads)/(total reads) * 1,000,000.

CeRNA network analysis

The expression levels of lncRNAs, miRNAs, and mRNAs differed significantly between APP/PS1 and WT mice. We searched the sequences of the lncRNAs and mRNAs to identify potential MREs. We used miRanda (http://www.microrna.org/microrna/) to predict miRNA-binding seed-sequence sites, and the presence of the same miRNA-binding sites in both lncRNAs and mRNAs indicated potential lncRNA–miRNA–mRNA interaction.

GO annotations and KEGG pathway analyses

The DAVID (https://david.ncifcrf.gov/summary.jsp) database was used to analyze lncRNA-miRNA-enriched genes. GO and KEGG terms with p values less than 0.05 were considered significantly enriched.

Construction of lncRNA-associated ceRNA networks

The lncRNA-associated ceRNA networks were constructed and visually displayed by using Cytoscape software V3.5.0 (San Diego, CA, USA) based on the analysis of high-throughput sequencing data, as described above. In the figures, distinct shapes and colors are used to represent different RNA types, and regulatory relationships.

Real-time qPCR validation

Total RNA was extracted by using TRIzol reagent (Sigma) according to the manufacturer's protocol. RNA quantity was measured by using a NanoDrop 2000 (Thermo Fisher Scientific). Quantitative RT-PCR was performed by using the GoScript™ Reverse Transcription System (Promega), in a C1000 Thermal Cycler (Bio-Rad). The glyceraldehyde-3-phosphate dehydrogenase gene (*Gapdh*) and U6 were used as an

internal control. Relative gene-expression levels were calculated using the $2^{-\Delta Ct}$ method (n=3).

Statistical analysis

Two normally distributed groups were compared by using *t* tests. Parameters for the high-throughput sequencing-related data were calculated, and statistical computing was performed by using R software. All data are expressed as means ± SD; a value of $p < 0.05$ was considered statistically significant.

Data access

All raw and processed sequencing data generated in this study have been submitted to the NCBI Gene Expression Omnibus (GEO; http://www.ncbi.nlm.nih.gov/geo/) under accession number GSE132177.

AUTHOR CONTRIBUTIONS

JW, WZ, and NM designed the study. NM, CT and BY participated in the animal experiments including tissue collection and RNA/protein extraction. NM performed the experiments and analyzed the data. NM, JW, and WZ analyzed the results and wrote the manuscript. All authors read and approved the final manuscript.

ACKNOWLEDGMENTS

We would like to thank the Shenzhen Biomedical Research Support Platform and the Shenzhen Molecular Diagnostic Platform of Dermatology for technical help.

CONFLICTS OF INTEREST

The authors declare that there are no conflicts of interest.

FUNDING

This work was supported by National Key R&D Program of China Grant 2016YFA0501903, National Natural Scientific Foundation of China (Grant No. 81571043 and 81673053), Natural Scientific Foundation of Guangdong Province (2016A030312016) and Shenzhen Basic Research Grants (JCYJ20160229153100269, JCYJ20170411090739316, JCYJ20170815153617033, JCYJ20180507182657867, JCYJ20170306161450254 and JCYJ20170306161807726).

REFERENCES

1. Neuman MA, Cohn R. Prevalence and malignancy of Alzheimer disease. Arch Neurol. 1976; 33:730. https://doi.org/10.1001/archneur.1976.00500100064022 PMID:973815

2. Zádori D, Veres G, Szalárdy L, Klivényi P, Vécsei L. Alzheimer's Disease: Recent Concepts on the Relation of Mitochondrial Disturbances, Excitotoxicity, Neuroinflammation, and Kynurenines. J Alzheimers Dis. 2018; 62:523–47. https://doi.org/10.3233/JAD-170929 PMID:29480191

3. Rosenbloom KR, Dreszer TR, Long JC, Malladi VS, Sloan CA, Raney BJ, Cline MS, Karolchik D, Barber GP, Clawson H, Diekhans M, Fujita PA, Goldman M, et al. ENCODE whole-genome data in the UCSC Genome Browser: update 2012. Nucleic Acids Res. 2012; 40:D912–17. https://doi.org/10.1093/nar/gkr1012 PMID:22075998

4. ENCODE Project Consortium. An integrated encyclopedia of DNA elements in the human genome. Nature. 2012; 489:57–74. https://doi.org/10.1038/nature11247 PMID:22955616

5. Eddy SR. Non-coding RNA genes and the modern RNA world. Nat Rev Genet. 2001; 2:919–29. https://doi.org/10.1038/35103511 PMID:11733745

6. Esteller M. Non-coding RNAs in human disease. Nat Rev Genet. 2011; 12:861–74. https://doi.org/10.1038/nrg3074 PMID:22094949

7. Chouliaras L, Rutten BP, Kenis G, Peerbooms O, Visser PJ, Verhey F, van Os J, Steinbusch HW, van den Hove DL. Epigenetic regulation in the pathophysiology of Alzheimer's disease. Prog Neurobiol. 2010; 90:498–510. https://doi.org/10.1016/j.pneurobio.2010.01.002 PMID:20097254

8. De Smaele E, Ferretti E, Gulino A. MicroRNAs as biomarkers for CNS cancer and other disorders. Brain Res. 2010; 1338:100–11. https://doi.org/10.1016/j.brainres.2010.03.103 PMID:20380821

9. Faghihi MA, Modarresi F, Khalil AM, Wood DE, Sahagan BG, Morgan TE, Finch CE, St Laurent G 3rd, Kenny PJ, Wahlestedt C. Expression of a noncoding RNA is elevated in Alzheimer's disease and drives rapid feed-forward regulation of beta-secretase. Nat Med. 2008; 14:723–30. https://doi.org/10.1038/nm1784 PMID:18587408

10. Khorkova O, Hsiao J, Wahlestedt C. Basic biology and therapeutic implications of lncRNA. Adv Drug Deliv Rev. 2015; 87:15–24. https://doi.org/10.1016/j.addr.2015.05.012 PMID:26024979

11. Martiskainen H, Haapasalo A, Kurkinen KM, Pihlajamäki J, Soininen H, Hiltunen M. Targeting ApoE4/ApoE receptor LRP1 in Alzheimer's disease. Expert Opin Ther Targets. 2013; 17:781–94.

https://doi.org/10.1517/14728222.2013.789862 PMID:23573918

12. Mercer TR, Mattick JS. Structure and function of long noncoding RNAs in epigenetic regulation. Nat Struct Mol Biol. 2013; 20:300–07. https://doi.org/10.1038/nsmb.2480 PMID:23463315

13. Mercer TR, Dinger ME, Mattick JS. Long non-coding RNAs: insights into functions. Nat Rev Genet. 2009; 10:155–59. https://doi.org/10.1038/nrg2521 PMID:19188922

14. Bond AM, Vangompel MJ, Sametsky EA, Clark MF, Savage JC, Disterhoft JF, Kohtz JD. Balanced gene regulation by an embryonic brain ncRNA is critical for adult hippocampal GABA circuitry. Nat Neurosci. 2009; 12:1020–27. https://doi.org/10.1038/nn.2371 PMID:19620975

15. Tripathi V, Ellis JD, Shen Z, Song DY, Pan Q, Watt AT, Freier SM, Bennett CF, Sharma A, Bubulya PA, Blencowe BJ, Prasanth SG, Prasanth KV. The nuclear-retained noncoding RNA MALAT1 regulates alternative splicing by modulating SR splicing factor phosphorylation. Mol Cell. 2010; 39:925–38. https://doi.org/10.1016/j.molcel.2010.08.011 PMID:20797886

16. Bernard D, Prasanth KV, Tripathi V, Colasse S, Nakamura T, Xuan Z, Zhang MQ, Sedel F, Jourdren L, Coulpier F, Triller A, Spector DL, Bessis A. A long nuclear-retained non-coding RNA regulates synaptogenesis by modulating gene expression. EMBO J. 2010; 29:3082–93. https://doi.org/10.1038/emboj.2010.199 PMID:20729808

17. Kallen AN, Zhou XB, Xu J, Qiao C, Ma J, Yan L, Lu L, Liu C, Yi JS, Zhang H, Min W, Bennett AM, Gregory RI, et al. The imprinted H19 lncRNA antagonizes let-7 microRNAs. Mol Cell. 2013; 52:101–12. https://doi.org/10.1016/j.molcel.2013.08.027 PMID:24055342

18. Wang Y, Xu Z, Jiang J, Xu C, Kang J, Xiao L, Wu M, Xiong J, Guo X, Liu H. Endogenous miRNA sponge lincRNA-RoR regulates Oct4, Nanog, and Sox2 in human embryonic stem cell self-renewal. Dev Cell. 2013; 25:69–80. https://doi.org/10.1016/j.devcel.2013.03.002 PMID:23541921

19. Cesana M, Cacchiarelli D, Legnini I, Santini T, Sthandier O, Chinappi M, Tramontano A, Bozzoni I. A long noncoding RNA controls muscle differentiation by functioning as a competing endogenous RNA. Cell. 2011; 147:358–69. https://doi.org/10.1016/j.cell.2011.09.028 PMID:22000014

20. Tay Y, Rinn J, Pandolfi PP. The multilayered complexity of ceRNA crosstalk and competition. Nature. 2014; 505:344–52. https://doi.org/10.1038/nature12986 PMID:24429633

21. Salmena L, Poliseno L, Tay Y, Kats L, Pandolfi PP. A ceRNA hypothesis: the Rosetta Stone of a hidden RNA language? Cell. 2011; 146:353–58. https://doi.org/10.1016/j.cell.2011.07.014 PMID:21802130

22. Rudenko A, Tsai LH. Epigenetic modifications in the nervous system and their impact upon cognitive impairments. Neuropharmacology. 2014; 80:70–82. https://doi.org/10.1016/j.neuropharm.2014.01.043 PMID:24495398

23. Mullane K, Williams M. Alzheimer's therapeutics: continued clinical failures question the validity of the amyloid hypothesis-but what lies beyond? Biochem Pharmacol. 2013; 85:289–305. https://doi.org/10.1016/j.bcp.2012.11.014 PMID:23178653

24. Jankowsky JL, Fadale DJ, Anderson J, Xu GM, Gonzales V, Jenkins NA, Copeland NG, Lee MK, Younkin LH, Wagner SL, Younkin SG, Borchelt DR. Mutant presenilins specifically elevate the levels of the 42 residue beta-amyloid peptide in vivo: evidence for augmentation of a 42-specific gamma secretase. Hum Mol Genet. 2004; 13:159–70. https://doi.org/10.1093/hmg/ddh019 PMID:14645205

25. Wang Z, Gerstein M, Snyder M. RNA-Seq: a revolutionary tool for transcriptomics. Nat Rev Genet. 2009; 10:57–63. https://doi.org/10.1038/nrg2484 PMID:19015660

26. Marguerat S, Bähler J. RNA-seq: from technology to biology. Cell Mol Life Sci. 2010; 67:569–79. https://doi.org/10.1007/s00018-009-0180-6 PMID:19859660

27. Kucherov G, Salikhov K, Tsur D. Approximate String Matching Using a Bidirectional Index. Data Structures and Algorithms. 2014. https://doi.org/10.1007/978-3-319-07566-2_23

28. Sun L, Luo H, Bu D, Zhao G, Yu K, Zhang C, Liu Y, Chen R, Zhao Y. Utilizing sequence intrinsic composition to classify protein-coding and long non-coding transcripts. Nucleic Acids Res. 2013; 41:e166. https://doi.org/10.1093/nar/gkt646 PMID:23892401

29. Kang YJ, Yang DC, Kong L, Hou M, Meng YQ, Wei L, Gao G. CPC2: a fast and accurate coding potential calculator based on sequence intrinsic features. Nucleic Acids Res. 2017; 45:W12–16. https://doi.org/10.1093/nar/gkx428 PMID:28521017

30. Mistry J, Bateman A, Finn RD. Predicting active site residue annotations in the Pfam database. BMC Bioinformatics. 2007; 8:298. https://doi.org/10.1186/1471-2105-8-298 PMID:17688688

31. Lin MF, Jungreis I, Kellis M. PhyloCSF: a comparative genomics method to distinguish protein coding and non-coding regions. Bioinformatics. 2011; 27:i275–82. https://doi.org/10.1093/bioinformatics/btr209 PMID:21685081

32. Langmead B, Salzberg SL. Fast gapped-read alignment with Bowtie 2. Nat Methods. 2012; 9:357–59. https://doi.org/10.1038/nmeth.1923 PMID:22388286

33. Wen M, Shen Y, Shi S, Tang T. miREvo: an integrative microRNA evolutionary analysis platform for next-generation sequencing experiments. BMC Bioinformatics. 2012; 13:140. https://doi.org/10.1186/1471-2105-13-140 PMID:22720726

34. Friedländer MR, Mackowiak SD, Li N, Chen W, Rajewsky N. miRDeep2 accurately identifies known and hundreds of novel microRNA genes in seven animal clades. Nucleic Acids Res. 2012; 40:37–52. https://doi.org/10.1093/nar/gkr688 PMID:21911355

35. Perry TL, Yong VW, Bergeron C, Hansen S, Jones K. Amino acids, glutathione, and glutathione transferase activity in the brains of patients with Alzheimer's disease. Ann Neurol. 1987; 21:331–36. https://doi.org/10.1002/ana.410210403 PMID:3579218

36. Lovell MA, Xie C, Markesbery WR. Decreased glutathione transferase activity in brain and ventricular fluid in Alzheimer's disease. Neurology. 1998; 51:1562–66. https://doi.org/10.1212/WNL.51.6.1562 PMID:9855502

37. Li L, Zi X, Hou D, Tu Q. Krüppel-like factor 4 regulates amyloid-β (Aβ)-induced neuroinflammation in Alzheimer's disease. Neurosci Lett. 2017; 643:131–37. https://doi.org/10.1016/j.neulet.2017.02.017 PMID:28189744

38. Schlüter A, Del Turco D, Deller T, Gutzmann A, Schultz C, Engelhardt M. Structural Plasticity of Synaptopodin in the Axon Initial Segment during Visual Cortex Development. Cereb Cortex. 2017; 27:4662–75. https://doi.org/10.1093/cercor/bhx208 PMID:28922860

39. Grigoryan G, Segal M. Ryanodine-mediated conversion of STP to LTP is lacking in synaptopodin-deficient mice. Brain Struct Funct. 2016; 221:2393–97. https://doi.org/10.1007/s00429-015-1026-7 PMID:25772508

40. Zhang XL, Pöschel B, Faul C, Upreti C, Stanton PK, Mundel P. Essential role for synaptopodin in dendritic spine plasticity of the developing hippocampus. J Neurosci. 2013; 33:12510–18. https://doi.org/10.1523/JNEUROSCI.2983-12.2013 PMID:23884954

41. Vlachos A, Ikenberg B, Lenz M, Becker D, Reifenberg K, Bas-Orth C, Deller T. Synaptopodin regulates denervation-induced homeostatic synaptic plasticity. Proc Natl Acad Sci USA. 2013; 110:8242–47. https://doi.org/10.1073/pnas.1213677110 PMID:23630268

42. Segal M, Vlachos A, Korkotian E. The spine apparatus, synaptopodin, and dendritic spine plasticity. Neuroscientist. 2010; 16:125–31. https://doi.org/10.1177/1073858409355829 PMID:20400711

43. Ufer C, Wang CC, Fähling M, Schiebel H, Thiele BJ, Billett EE, Kuhn H, Borchert A. Translational regulation of glutathione peroxidase 4 expression through guanine-rich sequence-binding factor 1 is essential for embryonic brain development. Genes Dev. 2008; 22:1838–50. https://doi.org/10.1101/gad.466308 PMID:18593884

44. Zhang S, Qin C, Cao G, Xin W, Feng C, Zhang W. Systematic Analysis of Long Noncoding RNAs in the Senescence-accelerated Mouse Prone 8 Brain Using RNA Sequencing. Mol Ther Nucleic Acids. 2016; 5:e343. https://doi.org/10.1038/mtna.2016.57 PMID:27483026

45. Zhang S, Qin C, Cao G, Guo L, Feng C, Zhang W. Genome-wide analysis of DNA methylation profiles in a senescence-accelerated mouse prone 8 brain using whole-genome bisulfite sequencing. Bioinformatics. 2017; 33:1591–95. https://doi.org/10.1093/bioinformatics/btx040 PMID:28130229

46. Guil S, Esteller M. RNA-RNA interactions in gene regulation: the coding and noncoding players. Trends Biochem Sci. 2015; 40:248–56. https://doi.org/10.1016/j.tibs.2015.03.001 PMID:25818326

47. Bartel DP. Metazoan MicroRNAs. Cell. 2018; 173:20–51. https://doi.org/10.1016/j.cell.2018.03.006 PMID:29570994

48. Denzler R, Agarwal V, Stefano J, Bartel DP, Stoffel M. Assessing the ceRNA hypothesis with quantitative measurements of miRNA and target abundance. Mol Cell. 2014; 54:766–76. https://doi.org/10.1016/j.molcel.2014.03.045 PMID:24793693

49. Cao X, Yeo G, Muotri AR, Kuwabara T, Gage FH. Noncoding RNAs in the mammalian central nervous system. Annu Rev Neurosci. 2006; 29:77–103. https://doi.org/10.1146/annurev.neuro.29.051605.112839 PMID:16776580

50. Xu B, Hsu PK, Stark KL, Karayiorgou M, Gogos JA. Derepression of a neuronal inhibitor due to miRNA dysregulation in a schizophrenia-related microdeletion. Cell. 2013; 152:262–75. https://doi.org/10.1016/j.cell.2012.11.052 PMID:23332760

51. Karreth FA, Reschke M, Ruocco A, Ng C, Chapuy B, Léopold V, Sjoberg M, Keane TM, Verma A, Ala U, Tay Y, Wu D, Seitzer N, et al. The BRAF pseudogene functions as a competitive endogenous RNA and induces lymphoma in vivo. Cell. 2015; 161:319–32. https://doi.org/10.1016/j.cell.2015.02.043 PMID:25843629

52. Taulli R, Loretelli C, Pandolfi PP. From pseudo-ceRNAs to circ-ceRNAs: a tale of cross-talk and competition. Nat Struct Mol Biol. 2013; 20:541–43. https://doi.org/10.1038/nsmb.2580 PMID:23649362

53. Sumazin P, Yang X, Chiu HS, Chung WJ, Iyer A, Llobet-Navas D, Rajbhandari P, Bansal M, Guarnieri P, Silva J, Califano A. An extensive microRNA-mediated network of RNA-RNA interactions regulates established oncogenic pathways in glioblastoma. Cell. 2011; 147:370–81. https://doi.org/10.1016/j.cell.2011.09.041 PMID:22000015

54. Tay Y, Kats L, Salmena L, Weiss D, Tan SM, Ala U, Karreth F, Poliseno L, Provero P, Di Cunto F, Lieberman J, Rigoutsos I, Pandolfi PP. Coding-independent regulation of the tumor suppressor PTEN by competing endogenous mRNAs. Cell. 2011; 147:344–57. https://doi.org/10.1016/j.cell.2011.09.029 PMID:22000013

55. Cai Y, Sun Z, Jia H, Luo H, Ye X, Wu Q, Xiong Y, Zhang W, Wan J. *Rpph1* Upregulates CDC42 Expression and Promotes Hippocampal Neuron Dendritic Spine Formation by Competing with miR-330-5p. Front Mol Neurosci. 2017; 10:27. https://doi.org/10.3389/fnmol.2017.00027 PMID:28223918

56. Nishizuka M, Kishimoto K, Kato A, Ikawa M, Okabe M, Sato R, Niida H, Nakanishi M, Osada S, Imagawa M. Disruption of the novel gene fad104 causes rapid postnatal death and attenuation of cell proliferation, adhesion, spreading and migration. Exp Cell Res. 2009; 315:809–19. https://doi.org/10.1016/j.yexcr.2008.12.013 PMID:19138685

57. Mochida GH, Mahajnah M, Hill AD, Basel-Vanagaite L, Gleason D, Hill RS, Bodell A, Crosier M, Straussberg R, Walsh CA. A truncating mutation of TRAPPC9 is associated with autosomal-recessive intellectual disability and postnatal microcephaly. Am J Hum Genet. 2009; 85:897–902. https://doi.org/10.1016/j.ajhg.2009.10.027 PMID:20004763

58. Fernandez RF, Kim SQ, Zhao Y, Foguth RM, Weera MM, Counihan JL, Nomura DK, Chester JA, Cannon JR, Ellis JM. Acyl-CoA synthetase 6 enriches the neuroprotective omega-3 fatty acid DHA in the brain. Proc Natl Acad Sci USA. 2018; 115:12525–30. https://doi.org/10.1073/pnas.1807958115 PMID:30401738

59. Poy MN, Eliasson L, Krutzfeldt J, Kuwajima S, Ma X, Macdonald PE, Pfeffer S, Tuschl T, Rajewsky N, Rorsman P, Stoffel M. A pancreatic islet-specific microRNA regulates insulin secretion. Nature. 2004; 432:226–30. https://doi.org/10.1038/nature03076 PMID:15538371

60. Gaughwin P, Ciesla M, Yang H, Lim B, Brundin P. Stage-specific modulation of cortical neuronal development by Mmu-miR-134. Cereb Cortex. 2011; 21:1857–69. https://doi.org/10.1093/cercor/bhq262 PMID:21228099

61. Shioya M, Obayashi S, Tabunoki H, Arima K, Saito Y, Ishida T, Satoh J. Aberrant microRNA expression in the brains of neurodegenerative diseases: miR-29a decreased in Alzheimer disease brains targets neurone navigator 3. Neuropathol Appl Neurobiol. 2010; 36:320–30. https://doi.org/10.1111/j.1365-2990.2010.01076.x PMID:20202123

62. Roshan R, Ghosh T, Gadgil M, Pillai B. Regulation of BACE1 by miR-29a/b in a cellular model of Spinocerebellar Ataxia 17. RNA Biol. 2012; 9:891–99. https://doi.org/10.4161/rna.19876 PMID:22664922

63. Figliuzzi M, Marinari E, De Martino A. MicroRNAs as a selective channel of communication between competing RNAs: a steady-state theory. Biophys J. 2013; 104:1203–13. https://doi.org/10.1016/j.bpj.2013.01.012 PMID:23473503

64. Guttman M, Russell P, Ingolia NT, Weissman JS, Lander ES. Ribosome profiling provides evidence that large noncoding RNAs do not encode proteins. Cell. 2013; 154:240–51. https://doi.org/10.1016/j.cell.2013.06.009 PMID:23810193

65. Nelson BR, Makarewich CA, Anderson DM, Winders BR, Troupes CD, Wu F, Reese AL, McAnally JR, Chen X,

Kavalali ET, Cannon SC, Houser SR, Bassel-Duby R, Olson EN. A peptide encoded by a transcript annotated as long noncoding RNA enhances SERCA activity in muscle. Science. 2016; 351:271–75. https://doi.org/10.1126/science.aad4076 PMID:26816378

66. Matsumoto A, Pasut A, Matsumoto M, Yamashita R, Fung J, Monteleone E, Saghatelian A, Nakayama KI, Clohessy JG, Pandolfi PP. mTORC1 and muscle regeneration are regulated by the LINC00961-encoded SPAR polypeptide. Nature. 2017; 541:228–32. https://doi.org/10.1038/nature21034 PMID:28024296

67. Anderson DM, Anderson KM, Chang CL, Makarewich CA, Nelson BR, McAnally JR, Kasaragod P, Shelton JM, Liou J, Bassel-Duby R, Olson EN. A micropeptide encoded by a putative long noncoding RNA regulates muscle performance. Cell. 2015; 160:595–606. https://doi.org/10.1016/j.cell.2015.01.009 PMID:25640239

68. Huang JZ, Chen M, Chen D, Gao XC, Zhu S, Huang H, Hu M, Zhu H, Yan GR. A Peptide Encoded by a Putative lncRNA HOXB-AS3 Suppresses Colon Cancer Growth. Mol Cell. 2017; 68:171–184.e6. https://doi.org/10.1016/j.molcel.2017.09.015 PMID:28985503

69. Trapnell C, Williams BA, Pertea G, Mortazavi A, Kwan G, van Baren MJ, Salzberg SL, Wold BJ, Pachter L. Transcript assembly and quantification by RNA-Seq reveals unannotated transcripts and isoform switching during cell differentiation. Nat Biotechnol. 2010; 28:511–15. https://doi.org/10.1038/nbt.1621 PMID:20436464

SUPPLEMENTARY MATERIALS

Supplementary Methods

MIRNA Methods

RNA isolation, quantification and qualification

RNA degradation and contamination was monitored on 1% agarose gels. RNA purity was checked using the Nano Photometer® spectrophotometer (IMPLEN, CA, USA). RNA concentration was measured using Qubit® RNA Assay Kit in Qubit® 2.0 Flurometer (Life Technologies, CA, USA). RNA integrity was assessed using the RNA Nano 6000 Assay Kit of the Bioanalyzer 2100 system (Agilent Technologies, CA, USA).

Library preparation for small RNA sequencing

A total amount of 3 μg total RNA per sample was used as input material for the small RNA library. Sequencing libraries were generated using NEBNext® Multiplex Small RNA Library Prep Set for Illumina® (NEB, USA.) following manufacturer's recommendations and index codes were added to attribute sequences to each sample. Briefly, NEB 3' SR Adaptor was directly, and specifically ligated to 3' end of miRNA, siRNA and piRNA. After the 3' ligation reaction, the SR RT Primer hybridized to the excess of 3' SR Adaptor (that remained free after the 3' ligation reaction) and transformed the single-stranded DNA adaptor into a double-stranded DNA molecule. This step is important to prevent adaptor-dimer formation, besides, dsDNAs are not substrates for ligation mediated by T4 RNA Ligase 1 and therefore do not ligate to the 5´ SR Adaptor in the subsequent ligation step. 5´ends adapter was ligated to 5´ends of miRNAs, siRNA and piRNA. Then first strand cDNA was synthesized using M-MuLV Reverse Transcriptase (RNase H–). PCR amplification was performed using LongAmp Taq 2X Master Mix, SR Primer for illumina and index (X) primer. PCR products were purified on a 8% polyacrylamide gel (100V, 80 min). DNA fragments corresponding to 140~160 bp (the length of small noncoding RNA plus the 3' and 5' adaptors) were recovered and dissolved in 8 μL elution buffer. At last, library quality was assessed on the Agilent Bioanalyzer 2100 system using DNA High Sensitivity Chips.

Clustering and sequencing

The clustering of the index-coded samples was performed on a cBot Cluster Generation System using TruSeq SR Cluster Kit v3-cBot-HS (Illumia) according to the manufacturer's instructions. After cluster generation, the library preparations were sequenced on an Illumina Hiseq 2500/2000 platform and 50bp.

Data analysis

Quality control

Raw data (raw reads) of fastq format were firstly processed through custom perl and python scripts. In this step, clean datas(clean reads) were obtained by removing reads containing ploy-N, with 5′ adapter contaminants, without 3′ adapter or the insert tag, containing ploy A or T or G or C and low quality reads from raw data. At the same time, Q20, Q30, and GC-content of the raw datas were calculated. Then, chose a certain range of length from clean reads to do all the downstream analyses.

Reads mapping to the reference sequence

The small RNA tags were mapped to reference sequence by Bowtie (Langmead et al. 2009) without mismatch to analyze their expression and distribution on the reference.

Known miRNA alignment

Mapped small RNA tags were used to looking for known miRNA. miRBase20.0 was used as reference, modified software mirdeep2 (Friedlander et al. 2011) and srna-tools-cli were used to obtain the potential miRNA and draw the secondary structures. Custom scripts were used to obtain the miRNA counts as well as base bias on the first position of identified miRNA with certain length and on each position of all identified miRNA respectively.

Remove tags from these sources

To remove tags originating from protein-coding genes, repeat sequences, rRNA, tRNA, snRNA, and snoRNA, small RNA tags were mapped to RepeatMasker, Rfam database or those types of datas from the specified species itself.

Novel miRNA prediction

The characteristics of hairpin structure of miRNA precursor can be used to predict novel miRNA. The available software miREvo (Wen et al. 2012) and mirdeep2 (Friedlander et al. 2011) were integrated to predict novel miRNA through exploring the secondary structure, the Dicer cleavage site and the minimum free energy of the small RNA tags unannotated in the former steps. At the same time, custom scripts were used to obtain the identified miRNA counts as well as base bias

on the first position with certain length and on each position of all identified miRNA respectively.

Small RNA annotation summary

Summarizing all alignments and annotations obtained before. In the alignment and annotation before, some small RNA tags may be mapped to more than one category. To make every unique small RNA mapped to only one annotation, we follow the following priority rule: known miRNA > rRNA > tRNA > snRNA > snoRNA > repeat > gene > NAT-siRNA > gene > novel miRNA > ta-siRNA. The total rRNA proportion was used a marker as sample quality indicator. Usually it should be less than 60% in plant samples and 40% in animal samples as high quality.

miRNA editing analysis

Position 2~8 of a mature miRNA were called seed region which were highly conserved. The target of a miRNA might be different with the changing of nucleotides in this region. In our analysis pipeline, miRNA which might have base edit could be detected by aligning all the sRNA tags to mature miRNA, allowing one mismatch.

miRNA family analysis

Exploring the occurrence of miRNA families identified from the samples in other species. In our analysis pipeline, known miRNA used miFam.dat (http://www.mirbase.org/ftp.shtml) to look for families; novel miRNA precursor was submitted to Rfam (http://rfam.sanger.ac.uk/search/) to look for Rfam families.

Target gene prediction

Predicting the target gene of miRNA was performed by miRanda (Enright et al, 2003) for animals.

Quantification of miRNA

miRNA expression levels were estimated by TPM (transcript per million) through the following criteria (Zhou et al. 2010): Normalization formula: Normalized expression = mapped readcount/Total reads*1000000

Differential expression of miRNA

For the samples with biological replicates: Differential expression analysis of two conditions/groups was performed using the DESeq R package (1.8.3). The P-values was adjusted using the Benjamini and Hochberg method. Corrected P-value of 0.05 was set as the threshold for significantly differential expression by default.

LNCRNA AND MRNA Methods

RNA isolation, quantification and qualification

RNA degradation and contamination was monitored on 1% agarose gels. RNA purity was checked using the Nano Photometer® spectrophotometer (IMPLEN, CA, USA). RNA concentration was measured using Qubit® RNA Assay Kit in Qubit® 2.0 Flurometer (Life Technologies, CA, USA). RNA integrity was assessed using the RNA Nano 6000 Assay Kit of the Bioanalyzer 2100 system (Agilent Technologies, CA, USA).

Library preparation for lncRNA sequencing

A total amount of 3 μg RNA per sample was used as input material for the RNA sample preparations. Firstly, ribosomal RNA was removed by Epicentre Ribo-zero™ rRNA Removal Kit (Epicentre, USA), and rRNA free residue was cleaned up by ethanol precipitation. Subsequently, sequencing libraries were generated using the rRNA-depleted RNA by NEBNext® Ultra™ Directional RNA Library Prep Kit for Illumina® (NEB, USA) following manufacturer's recommendations. Briefly, fragmentation was carried out using divalent cations under elevated temperature in NEBNext First Strand Synthesis Reaction Buffer(5X). First strand cDNA was synthesized using random hexamer primer and M-MuLV Reverse Transcriptase(RNaseH-). Second strand cDNA synthesis was subsequently performed using DNA Polymerase I and RNase H. In the reaction buffer, dNTPs with dTTP were replaced by dUTP. Remaining overhangs were converted into blunt ends via exonuclease/polymerase activities. After adenylation of 3′ ends of DNA fragments, NEBNext Adaptor with hairpin loop structure were ligated to prepare for hybridization. In order to select cDNA fragments of preferentially 150~200 bp in length, the library fragments were purified with AMPure XP system (Beckman Coulter, Beverly, USA). Then 3 μl USER Enzyme (NEB, USA) was used with size-selected, adaptor-ligated cDNA at 37° C for 15 min followed by 5 min at 95°C before PCR. Then PCR was performed with Phusion High-Fidelity DNA polymerase, Universal PCR primers and Index (X) Primer. At last, products were purified (AMPure XP system) and library quality was assessed on the Agilent Bioanalyzer 2100 system.

Clustering and sequencing

The clustering of the index-coded samples was performed on a cBot Cluster Generation System using

TruSeq PE Cluster Kit v3-cBot-HS (Illumia) according to the manufacturer's instructions. After cluster generation, the libraries were sequenced on an Illumina Hiseq 4000 platform and 150 bp paired-end reads were generated.

Data analysis

Quality control

Raw data(raw reads) of fastq format were firstly processed through in-house perl scripts. In this step, clean data(clean reads) were obtained by removing reads containing adapter, reads on containing ploy-N and low quality reads from raw data. At the same time, Q20, Q30 and GC content of the clean data were calculated. All the down stream analyses were based on the clean data with high quality.

Mapping to the reference genome

Reference genome and gene model annotation files were downloaded from genome website directly. Index of the reference genome was built using bowtie2 v2.2.8 and paired-end clean reads were aligned to the reference genome using HISAT2 (Langmead et al.) v2.0.4. HISAT2 was run with '--rna-strandness RF', other parameters were set as default.

Transcriptome assembly

The mapped reads of each sample were assembled by StringTie (v1.3.1) (Mihaela Pertea et al. 2016) in a reference-based approach. StringTie uses a novel network flow algorithm as well as an optional de novo assembly step to assemble and quantitate full-length transcripts representing multiple splice variants for each gene locus.

Coding potential analysis

CNCI

CNCI (Coding-Non-Coding-Index) (v2) profiles adjoining nucleotide triplets to effectively distinguish protein-coding and non-coding sequences independent of known annotations (Sun et al. 2013). We use CNCI with default parameters.

CPC

CPC (Coding Potential Calculator) (0.9-r2) mainly through assess the extent and quality of the ORF in a transcript and search the sequences with known protein sequence database to clarify the coding and non-coding transcripts (Kong et al. 2007). We used the NCBI eukaryotes' protein database and set the e-value '1e-10' in our analysis.

Pfam-sca

We translated each transcript in all three possible frames and used Pfam Scan (v1.3) to identify occurrence of any of the known protein family domains documented in the Pfam database (release 27; used both Pfam A and Pfam B) （Punta et al. 2012）. Any transcript with a Pfam hit would be excluded in following steps. Pfam searches use default parameters of -E 0.001 --domE 0.001 (Bateman et al. 2002).

PhyloCSF

PhyloCSF (phylogenetic codon substitution frequency) (v20121028) examines evolutionary signatures characteristic to alignments of conserved coding regions, such as the high frequencies of synonymous codon substitutions and conservative amino acid substitutions, and the low frequencies of other missense and nonsense substitutions to distinguish protein-coding and non-coding transcripts (Lin et al. 2011). We build multi-species genome sequence alignments and run phyloCSF with default parameters. Transcripts predicted with coding potential by either/all of the four tools above were filtered out, and those without coding potential were our candidate set of lncRNAs.

Conservative analysis

Phast (v1.3) is a software package contains much of statistical programs, most used in phylogenetic analysis (Siepel, et al. 2005), and phastCons is a conservation scoring and identificating program of conserved elements. We used phyloFit to compute phylogenetic models for conserved and non-conserved regions among species and then gave the model and HMM transition parameters to phyloP to compute a set of conservation scores of lncRNA and coding genes.

Quantification of gene expression level

Cuffdiff (v2.1.1) was used to calculate FPKMs of both lncRNAs and coding genes in each sample (Trapnell C. et al. 2010). Gene FPKMs were computed by summing the FPKMs of transcripts in each gene group. FPKM means fragments per kilo-base of exon per million fragments mapped, calculated based on the length of the fragments and reads count mapped to this fragment.

Differential expression analysis

The Ballgown suite includes functions for interactive exploration of the transcriptome assembly, visualization of transcript structures and feature-specific abundances for each locus, and post-hoc annotation of assembled features to annotated features (Alyssa C. Frazee et al. 2014). Transcripts with an P-adjust <0.05 were assigned as differentially expressed. Cuffdiff provides statistical

routines for determining differential expression in digital transcript or gene expression data using a model based on the negative binomial distribution (Trapnell C et al. 2010). Transcripts with an P-adjust <0.05 were assigned as differentially expressed.

Supplementary References

1. Anders S, Huber W. Differential expression analysis for sequence count data. Genome Biol. 2010; 11:R106. https://doi.org/10.1186/gb-2010-11-10-r106 PMID:20979621
2. Alyssa C. Frazee, Geo Pertea, Andrew E. Jaffe, Ben Langmead, Steven L. Salzberg
3. Enright AJ, John B, Gaul U, Tuschl T, Sander C, Marks DS. MicroRNA targets in Drosophila. Genome Biol. 2003; 5:R1. https://doi.org/10.1186/gb-2003-5-1-r1 PMID:14709173
4. Friedländer MR, Mackowiak SD, Li N, Chen W, Rajewsky N. miRDeep2 accurately identifies known and hundreds of novel microRNA genes in seven animal clades. Nucleic Acids Res. 2012; 40:37–52. https://doi.org/10.1093/nar/gkr688 PMID:21911355
5. Leek JT. Flexible analysis of transcriptome assemblies with Ballgown. bioRxiv. 2014.
6. Langmead B, Trapnell C, Pop M, Salzberg SL. Ultrafast and memory-efficient alignment of short DNA sequences to the human genome. Genome Biol. 2009; 10:R25. https://doi.org/10.1186/gb-2009-10-3-r25 PMID:19261174
7. Kanehisa M, Araki M, Goto S, Hattori M, Hirakawa M, Itoh M, Katayama T, Kawashima S, Okuda S, Tokimatsu T, Yamanishi Y. KEGG for linking genomes to life and the environment. Nucleic Acids Res. 2008; 36:D480–84. https://doi.org/10.1093/nar/gkm882 PMID:18077471
8. Langfelder P, Horvath S. WGCNA: an R package for weighted correlation network analysis. BMC Bioinformatics. 2008; 9:559. https://doi.org/10.1186/1471-2105-9-559 PMID:19114008
9. Mao X, Cai T, Olyarchuk JG, Wei L. Automated genome annotation and pathway identification using the KEGG Orthology (KO) as a controlled vocabulary. Bioinformatics. 2005; 21:3787–93. https://doi.org/10.1093/bioinformatics/bti430 PMID:15817693
10. McKenna A, Hanna M, Banks E, Sivachenko A, Cibulskis K, Kernytsky A, Garimella K, Altshuler D, Gabriel S, Daly M, DePristo MA. The Genome Analysis Toolkit: a MapReduce framework for analyzing next-generation DNA sequencing data. Genome Res. 2010; 20:1297–303. https://doi.org/10.1101/gr.107524.110 PMID:20644199
11. Siepel A, Bejerano G, Pedersen JS, Hinrichs AS, Hou M, Rosenbloom K, Clawson H, Spieth J, Hillier LW, Richards S, Weinstock GM, Wilson RK, Gibbs RA, et al. Evolutionarily conserved elements in vertebrate, insect, worm, and yeast genomes. Genome Res. 2005; 15:1034–50. https://doi.org/10.1101/gr.3715005 PMID:16024819
12. Storey JD. The positive false discovery rate: A Bayesian interpretation and the q-value. Ann Stat. 2003; 31:2013–35. https://doi.org/10.1214/aos/1074290335
13. Trapnell C, Williams BA, Pertea G, Mortazavi A, Kwan G, van Baren MJ, Salzberg SL, Wold BJ, Pachter L. Transcript assembly and quantification by RNA-Seq reveals unannotated transcripts and isoform switching during cell differentiation. Nat Biotechnol. 2010; 28:511–5. https://doi.org/10.1038/nbt.1621 PMID:20436464
14. Wang L, Feng Z, Wang X, Wang X, Zhang X. DEGseq: an R package for identifying differentially expressed genes from RNA-seq data. Bioinformatics. 2010; 26:136–38. https://doi.org/10.1093/bioinformatics/btp612 PMID:19855105
15. Wen M, Shen Y, Shi S, Tang T. miREvo: an integrative microRNA evolutionary analysis platform for next-generation sequencing experiments. BMC Bioinformatics. 2012; 13:140. https://doi.org/10.1186/1471-2105-13-140 PMID:22720726
16. Wu HJ, Ma YK, Chen T, Wang M, Wang XJ. PsRobot: a web-based plant small RNA meta-analysis toolbox. Nucleic Acids Res. 2012; 40:W22–8. https://doi.org/10.1093/nar/gks554 PMID:22693224
17. Young MD, Wakefield MJ, Smyth GK, Oshlack A. goseq: Gene Ontology testing for RNA-seq datasets. (goseq) 2010.
18. Zhou L, Chen J, Li Z, Li X, Hu X, Huang Y, Zhao X, Liang C, Wang Y, Sun L, Shi M, Xu X, Shen F, et al. Integrated profiling of microRNAs and mRNAs: microRNAs located on Xq27.3 associate with clear cell renal cell carcinoma. PLoS One. 2010; 5:e15224. https://doi.org/10.1371/journal.pone.0015224 PMID:21253009

Supplementary Tables

Please browse Full Text version to see the data of Supplementary Tables 1, 2

Supplementary Table 1. Differentially expressed lncRNAs between the APP/PS1 and WT at 6 months.

Supplementary Table 2. Differentially expressed lncRNAs between the APP/PS1 and WT at 9 months.

Supplementary Table 3. Differentially expressed miRNAs between the APP/PS1 and WT at 6 months.

sRNA	AD_6m_readcount	WT_6m_readcount	log2FoldChange	pval	padj
mmu-miR-365-3p	198.708	304.0374	-0.57773	0.000318	0.083311
mmu-miR-193b-3p	112.1526	174.3495	-0.59548	0.000402	0.083311
mmu-miR-190a-5p	79.42082	128.3713	-0.63956	0.00069	0.095195
mmu-miR-467a-3p	4.755073	18.71602	-1.1506	0.00143	NA
mmu-miR-467d-3p	4.755073	18.71602	-1.1506	0.00143	NA
mmu-miR-7688-5p	2.024379	11.96322	-1.1013	0.002897	NA
mmu-miR-206-3p	31.80409	64.54004	-0.83853	0.002933	0.30361
mmu-miR-3068-3p	1194.228	1355.86	-0.18228	0.004847	0.34848
mmu-miR-135b-5p	798.43	967.9046	-0.27532	0.00505	0.34848
mmu-miR-466i-5p	1.893169	9.957711	-1.0196	0.005855	NA
mmu-miR-9b-5p	4140.593	3242.95	0.34171	0.006333	0.37457
mmu-miR-192-5p	2025.665	2292.821	-0.17723	0.008521	0.44096
mmu-miR-219b-5p	1662.885	1413.753	0.2303	0.009742	0.44812
mmu-miR-669f-3p	2.542842	9.358751	-0.93601	0.011302	NA
mmu-miR-219a-2-3p	9168.137	8113.984	0.17496	0.012751	0.5279
mmu-miR-449a-5p	14.8024	27.75103	-0.72572	0.012781	NA
mmu-miR-744-5p	2526.509	2127.922	0.24359	0.014179	0.53363
mmu-miR-6933-5p	0	3.107846	-0.78476	0.014817	NA
mmu-miR-128-2-5p	41.80851	65.26091	-0.57317	0.016213	0.55405
mmu-miR-128-3p	243732	324443.4	-0.39123	0.017398	0.55405
mmu-miR-138-5p	3620.765	4177.49	-0.20349	0.021657	0.64044
mmu-miR-540-3p	338.4309	392.9069	-0.21	0.023941	0.66078
mmu-miR-3058-5p	3.289875	0.230233	0.72575	0.024607	NA
mmu-miR-122-5p	23.5908	42.24209	-0.67852	0.025612	NA
mmu-miR-122b-3p	23.5908	42.24209	-0.67852	0.025612	NA
mmu-miR-339-3p	110.4606	85.54921	0.3446	0.026789	0.69317
mmu-miR-881-3p	33.25634	17.49266	0.68477	0.029711	NA
mmu-miR-22-5p	669.6717	587.3613	0.18432	0.032178	0.76762
mmu-miR-31-5p	160.4705	194.9269	-0.27158	0.033375	0.76762
mmu-miR-350-5p	27.90635	17.21211	0.5873	0.036007	NA
novel_423	0	2.210589	-0.62351	0.03829	NA
mmu-miR-3097-3p	2.292271	6.86052	-0.76217	0.039745	NA
mmu-miR-1983	423.094	335.3748	0.3224	0.04149	0.83571
mmu-miR-30b-5p	3417.078	3819.289	-0.15864	0.043612	0.83571
mmu-miR-450b-5p	17.6654	9.588984	0.65493	0.044437	NA
mmu-miR-369-5p	3361.434	2998.785	0.16292	0.046922	0.83571

Please browse Full Text version to see the data of Supplementary Tables 4–14

Supplementary Table 4. Differentially expressed miRNAs between the APP/PS1 and WT at 9 months.

Supplementary Table 5. Differentially expressed mRNAs between the APP/PS1 and WT at 6 months.

Supplementary Table 6. Differentially expressed mRNAs between the APP/PS1 and WT at 9 months.

Supplementary Table 7. Nodes interactions in the 6yes9no group (UP-DOWN-UP).

Supplementary Table 8. Nodes interactions in the 6yes9no group (DOWN-UP-DOWN).

Supplementary Table 9. Nodes interactions in the 6no9yes group (UP-DOWN-UP).

Supplementary Table 10. Nodes interactions in the 6no9yes group (DOWN-UP-DOWN).

Supplementary Table 11. Nodes interactions in the 6yes9yes group.

Supplementary Table 12. GO and KEGG pathways in the 6yes9no group.

Supplementary Table 13. GO and KEGG pathways in the 6no9yes group.

Supplementary Table 14. GO and KEGG pathways in the 6yes9yes group.